Volumetric Bioprinting for Medical Applications

Arturo López Franco

School of Engineering and Sciences
Insituto Tecnológico y de Estudios Superiores de Monterrey

This dissertation is submitted for the degree of
Master of Science in Engineering Science

June 2020

I would like to dedicate this thesis to my loving parents and brothers, thank you for your support and encouragement.

Acknowledgements

I would like to express my special thanks of gratitude to Dr. Cesar Vargas, Telecommunications Research Group Chair at Tecnológico de Monterrey, and Dr. Shrike Zhang, Assistant Professor at Harvard Medical School, my research supervisors, for their able guidance and support for completing this project.

I would also like to thank the team of Zhang Lab., for their practical and theoretical contribution to this project. I would like to extend my gratitude to Tecnológico de Monterrey support on tuition and CONACyT with the support for living.

This project was elaborated at Zhang Lab. Division of Engineering Living Systems of Brigham and Women's Hospital affiliation of Harvard Medical School.

Abstract

Additive manufacturing (3D printing) has been a widely used tool in a lot of different industries. Among these industries can be found tissue engineering and regenerative medicine, since bioprinting is one of the main techniques applied. The implementations of new technologies for additive manufacturing, have been adapted into the bioprinting area for medical purposes. Additive manufacturing technologies have been evolving from printing point-to-point, layer-by-layer, and more recently volumetric printing, which represents printing a whole volume simultaneously.

In this thesis is presented a new technique for bioprinting, the Computed Axial Lithography (CAL) printing, which is a recently additive manufacturing technology based on reconstructing a volume simultaneously, has demonstrated to have advantages against other additive manufacturing techniques, improving the printing speed, the resolution, minimum material waste, and more, and its application in the medicine industry has not been explorer looking very promising for this research field with limitless applications.

The bioink used in the experiments presented is a GelMA-based hydrogel, and the 3D structures achieved should be capable of present biocompatibility with living organisms.

For this thesis, the reproduction of the CAL printing for biomaterials, in this particular case GelMA, is proved, opening the doors for applying the same concept to different biomaterials, which could have limitless applications in many distinct research areas.

Table of contents

List of figures

List of tables

Chapter 1

Introduction

1.1 Background

In the United States (July 2019), more than 113,000 people are enrolled in the national transplant waiting list for a healthy organ [1]. Every ten minutes another person is added to the waiting list, each day 20 people die waiting for a transplant. Each year, the number of people on the waiting list continues to be much larger than both the number of donors and transplants, see figure 1.1 for more detail statistics about the organ donor shortage in the United States.

Tissue engineering has been a promising field of research, offering hope for reducing the gap between organ shortage and transplantation needs. Organ printing, which is defined as computer-aided additive biofabrication of 3D cellular tissue constructs, has shed light on advancing this field into a new era. Organ printing takes advantages of rapid prototyping (RP) technology to print cells, biomaterials, and cell-laden biomaterials, directly creating 3D tissue-like structures [8].

Bioprinting is a 3D fabrication technology used to precisely dispense cell-laden biomaterials for the construction of complex 3D functional living tissues or artificial organs. While still in its early stages, bioprinting strategies have demonstrated their potential use in regenerative medicine to generate a variety of transplantable tissues, including skin, cartilage, and bone [2].

Biofabrication technologies, including stereolithography and extrusion-based printing, are revolutionizing the creation of complex engineered tissues. The current paradigm in bioprinting relies on the additive layer-by-layer deposition and assembly of repetitive building blocks.

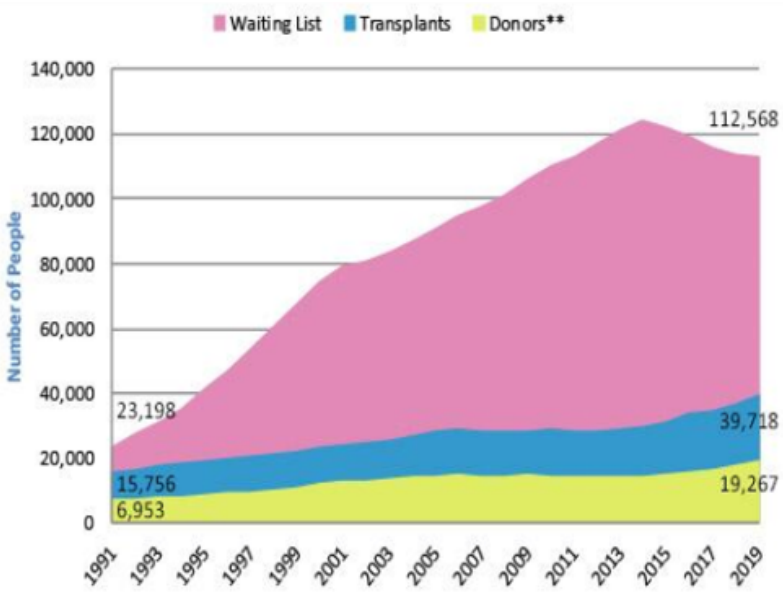

Figure 1.1: Organ donor shortage. Data from [1].

The scalability of these additive manufacturing technologies is limited by their printing velocity, as lengthy biofabrication processes impair cell functionality.

CAL printing also known as volumetric printing, is a technique capable of reconstruct structures based on the tomography concept, this permits the creation of geometrically complex, millimeter-scale constructs at an unprecedented printing velocity, opening new avenues for upscaling the production of hydrogel-based constructs and for their applications on tissue-engineering, regenerative medicine, and soft robotics [9]. The CAL printing technique applied to the medial industry has the potential to revolutionize the area of transplants, regenerative medicine and more.

1.2 Project Aim

The project aim is to design and develop a system capable to reproduce the CAL printing technique, focusing on the applications for hydrogels, in this case gelatin methacrylate (GelMa), to generate three-dimensional geometries in biomaterials capable of support living cells, utilizing visible light spectrum, for medical applications.

1.3 Justification

Multiple science areas are focused on finding a solution for the organ shortage crisis, to be able to eliminate or reduce the gap between patients waiting for an organ donor and the availability of organs, one of the principal areas with the potential to find a viable solution is the tissue engineering, specially focusing in the bioprinting. The results from this project has the potential to impact the tissue engineering and medicine regenerative areas, especially the projects related to 3D BioPrinting. This project has a lot of impact because it could decrease in time and cost the way the 3D bioprinting is normally done, making way to multiple medical applications.

Chapter 2

Review of Literature

2.1 Additive Manufacturing

Additive manufacturing (AM), is a technology that is rapidly developing and is being integrated into the manufacturing area, and our everyday lives [10]. It can be found with different names, such as three dimensional (3D) printing, rapid prototyping (RP), layer manufacturing (LM) or solid free-form fabrication. The basic principle of this technology is that a model, initially generated using a three-dimensional Computer-Aided Design (3D CAD) system, can be fabricated directly without the need for process planning. AM technology has developed over time as materials, accuracy, and the overall quality of the output improved.

As AM has been incorporated in industry, its global market has steadily increased since the first 3D printer was made. Due to this continuous exponential growth in interest, market, and adoption of technologies, additive manufacturing has been driving major innovations in many areas, such as engineer, manufacturing, art, education and medicine. Different technologies of AM have been made, each of them having advantages and disadvantages over the other. AM will continue to become more integrated into industry and our personal lives as the technology and availability continue to grow [11].

2.2 Tissue Engineering

Tissue Engineering (TE) is a promising option to address the shortage of organs availability. TE is a multidisciplinary field that combine chemistry, medicine, engineering, material science, pharmaceutics and more, to develop therapies and products for repair or replacement of damaged tissue and organs [12].

The process of Tissue Engineering is multistep and involves engineering of different components that will combine to generate the desired tissue or organ. Today, this field has advanced so much that it is being used to develop therapies for patients that have severe chronic disease affecting major organs, such as the kidney, heart and liver [13].

Other diseases or conditions that can benefit from TE technologies include skin burns, bone defect, nervous system repair, craniofacial reconstruction, cornea replacement, volumetric muscle loss, cartilage repair, vascular disease, pulmonary disease, gastrointestinal tissue repair, and cosmetic procedures [13].

Specific advancements that have benefited TE as a recent field in recent years include novel biomaterials, three dimensional bioprinting technologies, integration of nanotechnology, and gene-editing technology [14].

2.3 Introduction to Bioprinting

The introduction of additive manufacturing has impulsed a manufacturing revolution, and the medical sector is not staying behind, taking advantage of this technology in the field of biofabrication and tissue engineering.

AM has found numerous applications in many areas of biomedical research and clinical practice. Recently, improvements in bioengineering techniques and a substantial fall in price of equipment have meant that the use of 3D printing to create soft tissue, and organs has become an increasingly viable area of research [15], in addition, a variety of biomaterials are already available for 3D printing of live cells.

Bioprinting is a 3D fabrication technology used to precisely dispense cell-laden biomaterials for the construction of complex 3D functional living tissues or artificial organs. While still in its early stages, bioprinting strategies have demonstrated their potential use in regenerative medicine to generate a variety of transplants tissues, including skin, cartilage, and bone [2].

In bioprinting techniques, small units of cells and biomaterials are dispensed with precision to form tissue-like structures. Unlike conventional 3D printing techniques, bioprinting requires a different technical approach that is compatible with depositing living cells. The advantages of bioprinting include accurate control of cell distribution, high-resolution cell deposition, scalability, and cost-effectiveness.

To successfully create bioprinted tissues, it is necessary to generate the printing paths, select appropriate bioinks, control the bioprinter and perform quality control after printing [16]. The typical bioprinting process is a follows:

1. Design the printing geometry and verify its feasibility.
2. Select the appropriate cell types and hydrogels, which forms the bioink, and load it into the bioprinting system.
3. The design path is sent to the bioprinting system.
4. The bioprinter builds structures to form the designed geometry.
5. Bioprinted tissues are checked after bioprinting.

2.4 Bioprinting Techniques

Bioprinting technology shows potential in tissue engineering for the fabrication of scaffolds, cells, tissues and organs reproducibly with high accuracy. Bioprinting utilizes biomaterials, cells or cell factors as a bioink to fabricate prospective tissue structures [17].

Different bioprinting technologies applied different techniques, being all of them variations from existing additive manufacturing techniques, adapted to the medical area, being the main difference the material used and the corresponding modifications to work efficiently with the different bioinks. Some of the most current popular techniques are presented in this section, being these: inkjet bioprinting, laser-assisted bioprinting, extrusion bioprinting, and stereolitography, each of them have specific strengths, weakness, and limitations. A graphic representation of the printing technologies shown in this section can be seen in figure 2.1.

2.4.1 Inkjet Bioprinting

Inkjet bioprinting was the first bioprinting technology [18]. A hydrogel pre-polymer solution with encapsulated cells (bioink) is stored in the ink cartridge. The cartridge is then connected to a micro-electromechanical system (MEMS) based printer head and acts as the bioink source during the electronically controlled printing process. During printing, the printer heads are deformed by a thermal or piezoelectric actuator and squeezed to generate droplets of a controllable size. The advantages of inkjet printing include: low cost due to similar structure with commercial printers, high printing speed conferred by the ability of the printer head to support parallel work mode, and relatively high cell viability (usually from 80% to 90%) [2].

However, printer heads are not able to squeezed out high viscosity materials ($> 15 mPa/s$) and do not work well with bioinks with high cell density ($1x10^6 cells/ml$). High cell density increases the average viscosity of bioinks, resulting in clogging of the head [19]. Another disadvantage of inkjet printing is the settling effect [20]. When bioinks are initially loaded into the ink cartridge, the bioinks are well mixed, however, over the entire printing process, cells begin to settle in the cartridge, increasing the viscosity of the bioink and often clogging the printer head. Additionally the most common print heads and cartridges are not capable of storing enough bioink to print large tissues, limiting the applications of this bioprinter.

2.4.2 Laser-assisted Bioprinting

Laser-assisted bioprinting uses a laser as the energy source to deposit the bioink. With this technique, during printing, a focused laser pulse is applied to stimulate a small area of the absorbing layer. The critical part of the laser-assisted printing system is a donor layer that responds to laser stimulation. This laser pulse vaporizes a portion of the donor layer, creating a high-pressure bubble at the interface of the bioink layer and propelling the suspended bioink. The falling bioink droplet is collected on the receiving substrate and subsequently crosslinked [2].

Compare to inkjet printer, laser-assisted printing avoid direct contact between the dispenser and the bioinks, an advantage for a technique with no contact is that does not cause mechanical stress to the cells, which results in high cell viability (usually higher than 95%). In addition, laser-assisted printing can also print highly viscous materials (high cell density materials), resulting in more types of bioinks that can be used than in inkjet printing [21].

Laser diodes with high-resolution and intensity can be very expensive compared to other nozzle-based printing methods, and the control of the laser printing system can be found complicated, limiting the technique's adoption. In addition to the high equipment cost, laser-assisted printing is still immature because of unexplored parameters affecting the droplet size and quality.

2.4.3 Extrusion Bioprinting

Extrusion printing is a modification of inkjet printing. In order to print the viscous materials inkjet printers cannot deposit, extrusion printing uses either an air-force pump or mechanical screw plunger to dispense bioinks.

By applying a continuous force, extrusion printing can print uninterrupted cylindrical lines rather than a single bioink droplet. Almost, all types of hydrogel pre-polymer solutions of

varying viscosity as well aggregates with high cell density can be printed with extrusion bioprinters.

While extrusion bioprinters can print a wider range of materials, they also expose encapsulated cells to a larger mechanical stresses that are thought to reduce cell viability [16]. Pneumatic micro nozzles powered by compressed gases support a wider range of viscosity, but have difficulty precisely controlling the deposited mass. Screw-based nozzles can print without inlet air and are much cheaper, but they experience problems in high viscosity dispensing.

2.4.4 Stereolitography

Stereolitography (SLA) is a system where ultra-violet (UV) light source is focused down into a UV photo-curable liquid polymer bath, where the polymer hardens. Uncured polymers stays in the bath and provides support to the part that is being built. After a layer of printing is done, the hardened layer polymer moves down on a build plate in the liquid medium, and the next layer of polymer is available on the top of the following layer. This process continues until the part is finished based on the CAD design and its removed from the liquid medium.

Stereolithography has also been modified for bioprinting purposes. Like laser-assisted printing, stereolithography bioprinters use light to selectively solidify a bioink in a layer-by-layer process that additively builds up objects [22]. These printers use a digital light projector to cure bioinks plane-by-plane and have several advantages over traditional bioprinting methods. No matter how complex pattern in one layer is, the printing time is the same because the entire pattern is projected over the printing plane. As a result, the printer only needs a moveable stage in vertical direction, which significantly simplifies the control of the printer.

2.5 Bioprinting Applications

The goal of tissue engineering is to fabricate 3D artificial tissues or organs composed of a scaffold, cells and a microenvironment that mimics the real environment of the human body. As a highly effective and accurate method to fabricate artificial tissue in vitro, printing achieves these three necessary components [17]. Different types of 3D printing are utilized for applications that range from studies of cellular behavior to investigations of tissue pharmacodynamics or toxicological mechanisms.

Being this, one of the areas with most rapidly growth, medical and egineering researchers from all areas have been working on different applications. 3D printing has been successfully

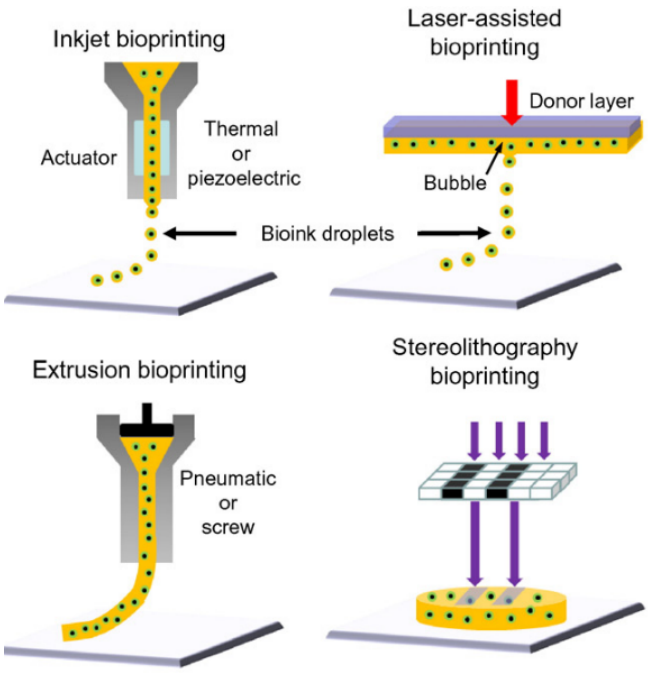

Figure 2.1: Most popular printing techniques [2].

used in the medical sector, making prosthetic limbs, repairing bones, and creating surgical implants, various human tissues have already been successfully printed including skin, liver, neuronal tissue, muscle-tendon units, cartilage and more. Next is presented as example some of the areas where bioprinting technologies have been successfully applied.

With the development of new technologies and materials, future applications and research for bioprinting are limitless, expecting to include the entire healthcare sector. Some bioprinting applications are shown in figure 2.2.

2.5.1 Vascular

Tissue engineered vascular grafts are a potential alternative source to blood vessel [16]. The development of a tissue-engineered blood vessel substitute has motivated much of the research in the area of cardiovascular tissue engineering overthe past 20 years [23]. Several methodologies have emerged for constructing blood vessel replacements with biological functionality. These include cell-seeded collagen gels, cell-seeded biodegradable synthetic polymer scaffolds, cell self-assembly, and acellular techniques. The availability of new biomaterials and ever-evolving printing methods offer hope that functional blood vessel structures and branched vascular networks may soon be accessible using a bioprinting

strategy. Bioprinting is an attractive approach, since it facilities the fabrication of constructs with tubular geometries using relative simple protocols and apparatus.

2.5.2 Organs

Additive manufacturing has also been used for fabrication of artificial organ replacements (prosthetics) and external deformity-correcting devices (orthotics). As far as prosthetics are concerned, AM could offer easy and affordable customization options not only to make the prosthetic device fit the anatomy of the patient but also to adjust functional aspects of the prosthetic device,

Additive Manufacturing has added a new dimension to the design and manufacturing of implants in general, and patient specific implants in particular. Patient-specific implants, where the implant is designed to fit the anatomy or other requirements of a single patient, are one of the principal areas for routine clinical application of additive manufacturing techniques [24].

2.5.3 Bone

The use of additive manufacturing technologies in bone engineering has been growing in the recent years. Among the different technology options, three dimensional printing is becoming popular due to the ability to directly print porous scaffolds with designed shape, controlled chemistry and interconnected porosity [25]. 3D printing technique, is the most sophisticated technique to produce scaffolds geometries, making it one of the best techniques to construct bone if the right material is applied. In [26] is demonstrated the feasibility of generating 3D printed scaffolds that induce osteogenic commitment of stem cells.

2.5.4 Organ-on-chip

Bioprinting has also been used to seed cell layers uniformly on each side of the interface of micro devices for the formation of organ-on-a-chip devices [27]. Organ-on- a-chip systems mimic parts of typical organ functions to investigate the interactions between drugs and their potential effects on tissues [28]. Bioprinting may play an important role in organ-on-a-chip technology, given it is a practical solution for the formation of uniform and highly controllable tissue layers at low cost [16].

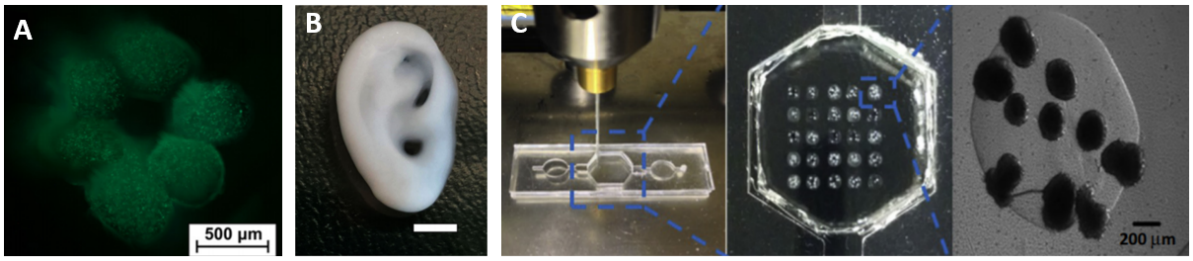

Figure 2.2: Bioprinting applications. A) In [3] is presented a vessel-like structure. B) In [4] is presented an ear structure created using bioink for cartilage bioprinting applications, scale bar 5mm. C) In [5] is presented a liver-on-a-chip for drug screening applications.

2.6 Materials for Bioprinting

The material selection remains a significant concern and limitation for bioprinting. Bioink can be considered the equivalent to "ink" or ABS plastics of a typical 3D printer, for a bioprinter. Bioinks typically consist of an hydrogel pre-polymer solution and cells previously cultivated in the polymers, to try to simulate tissue environment. A critical element in virtually all tissue engineering approaches is the polymer scaffold. The polymer potentially mimics many roles of extracellular matrixes found in tissues.

A current limitation is the limited availability of bioinks that possess appropriate physical properties for the printing process and simultaneously provide a suitable niche for the cells to differentiate towards the desired lineage [24].

An exciting alternative approach to cell delivery for tissue engineering is the use of polymers (i.e., hydrogels) that can be injected into the body. This approach enables to transplant the cell and polymer combination in a minimally invasive manner. Hydrogels have structural similarity to the macromolecular-based components in the body and are considered biocompatible [29].

Hydrogels have found numerous applications in tissue engineering as well as in drug delivery. Tissue engineering is the most recent application of hydrogels, in which they are used as scaffolds to engineer new tissues [30].

Hydrogels, currently used or with potential applications in tissue engineering, are divided into two categories, according to their natural or synthetic origin. Hydrogels from natural polymers have been widely used for tissue engineering approaches. However, limitations of gels from natural polymers have motivated approaches to modify these polymers as well as to use various synthetic polymers [31]. A wide range of synthetic polymers may potentially have suitable chemical and physical properties for these applications.

2.6.1 Hydrogels Characteristics

Hydrogels play an essential role in bioprinting. They not only have direct contact with cells to provide structural support, but they also dominate the chemical and physical properties of bioinks [32]. The desired application of the bioprinted structured consists directly of the type and characteristics of hydrogel used, this is the principal component of the bioinks.

Hydrogels in tissue engineering must meet a number of design criteria to work correctly, the criterial must include physical parameters, as well as biological parameters. Hydrogels should maintain sufficient mechanical properties after polymerization to provide the cells with a stable environment [33]. Mechanical properties are considered to be highly essential for soft tissue, such as cartilage and skin, because the functions of such tissues mainly rely on the mechanical properties [34].

Another important property of hydrogels used for bioinks, is the biocompatibility, biocompatibility refers to the ability of the material to perform with an appropriate host response in a specific situation [35]. For in vitro applications, biocompatibility requires that the material itself is not harmful to cells, and provides binding with the cells [32]. For in vivo applications, biocompatibility adds the requirement that the material can be degraded by or integrated the host.

2.6.2 Hydrogels from Natural Polymers

In this section is presented a couple of the most used hydrogels from natural polymers, in tissue engineering, collagen and gelatin, the polymer used in this project is related to these. Both of them have shown exceptional biocompatibilities characteristics with different human tissue.

Collagen

Collagen is the most widely used tissue-derived natural polymer, and it is the main component of extracellular matrices of mammalian tissues including skin, bone, cartilage, tendon, and ligament. These gels are still short of physical strength, potentially immunogenic, and can be expensive [36]. Collagen meets many of the biological design parameters, it is composed of specific combinations of amino acid sequences that are recognized by cells and degraded by enzymes secreted from the cells (i.e., collagenase). Collagen has been used as a tissue culture scaffold or artificial skin due to the ready attachment of many different cell types and its cell-based degradation.

Collagen gel has been utilized for reconstruction liver, skin, blood, vessel, and small intestine [37].

Gelatin

Gelatin is a derivated from Collagen, formed by breaking the natural triple-helix structure of collagen into single-strand molecules. It has been used in many tissue engineering applications due to its biocompatibility and ease of gelation. Gelatin gels have also been utilized for the delivery of growth factors to promote vascularization of engineered new tissue [38].

2.6.3 Hydrogels from Synthetic Polymers

These hydrogels are derived from the synthetic origin. Unlike the hydrogels derived from natural origin, these kind of hydrogels are not biocompatible nor degradable, but their properties can be modified to achieve design parameters, and mechanical characteristics. [31].

2.6.4 Gelatin Methacryloyl

Van Den Bulcke et al. generated photocrosslinkable gelatin derivatives by reacting gelatin with methacrylic anhydride (MA) [39]. The resulting material was termed as GelMA. The material selected for this experiment is GelMA, GelMA is one of the most popular hydrogels used for tissue engineering and medicine regenerative applications.

GelMA is synthetized by adding methacrylate groups to the amine-containing side-groups of gelatin, which becomes a photocrosslinkable hydrogel [40]. GelMA hydrogels carry advantages that are representative characters of both natural and synthetic biomaterials. The main component of GelMA is gelatin, which provides cell-responsive characteristics. Methacrylation and photocrosslinking provide mechanical and chemical properties, including the ability to create 3D architectures [41].

Among the characteristics that make GelMA one of the most popular hydrogels for tissue engineering, is that GelMA hydrogels are suitable for both two-dimensional (2D) cell seeding and three-dimensional (3D) cell encapsulation, compatible with various microfabrication techniques, tuneable in regards to their physical properties, cost efficiency, and easy to synthesize [42].

One important characteristic of GelMA is that can be photocrosslinked, meaning that the crosslinking can be initiated by a light source depending of the photoinitiator applied, when the crosslinked occur, the parts crosslinked in GelMA become solid, taking advantage of this characteristic for 3D formations [43] in a biocompatible material (biomaterial). Light-induced photocrosslinking has been widely used for the fabrication of cell-laden injectable hydrogels.

2.6.5 Cell Culture

Cell proliferation is needed in bioinks in order to mimic tissue or organ on a macroscale. Two main factors are considered when selecting cells for bioprinting: how closely the bioprinted cells can mimic the physiological state of cell in vivo, and what degree the bioprinted cells can maintain or develop their in vivo functions under optimized microenvironments [16].

Direct printing of primary cells can rapidly increase the complexity of the bioprinting. Traditional bioprinting techniques for printing different cell types required that the hydrogels with cells embedded be printed in parallel, to achieve this, many bioinks need to be prepared for each print.

In [44] is demonstrated that GelMA hydrogels can be adjusted to the intended application as a three-dimensional (3D) cell culture platform, providing the cells with an optimal biological environment. For clinical applications, cells for bioprinting would ideally be isolated from the patients themselves to avoid negative immune responses[8].

2.7 Beer-Lambert Law

When a monochromatic radiation beam, of intensity I_0 impacts perpendicular a substance inside a container able to absorb radiation, after the beam has traveled a distance L, the intensity decrease its value to I_1 as a consequence of the radiation absorption [45].

The Beer-Lambert law dictates the relationship between the transmitted light with the concentration of the substance c in the light beam trajectory, the longitude of the substance body the light gets through L and the probability that a photon can be absorbed by the material (molar absorption coefficient) ε [46].

The transmittance, shown in equation 2.1, is defined as a dimensionless quantity proportional to the distance a light beam can traveled in a body, and can take values between 0 and 1, where 1 indicates that the light can completely go through the body without any loss, and 0 that the light is unable to cross the material.

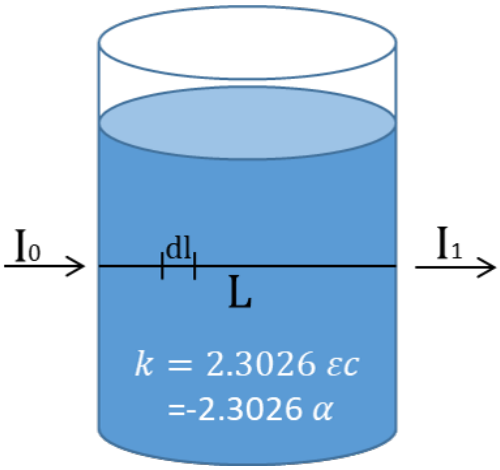

Figure 2.3: Beer-Lambert law.

$$T = I_1/I_0 = 10^{-A} \tag{2.1}$$

$$d_i/d_l = -k_i \tag{2.2}$$

$$\int_{I_0}^{I_1} d_i/i = -\int_0^l kdl \tag{2.3}$$

The result from solving equation 2.3 is expressed in equation 2.4, also known as absorbance as shown in equation 2.5.

$$log_{10}(I_0/I_1) = KL/2.3026 \tag{2.4}$$

$$A = log_{10}(I_0/I_1) = \varepsilon cL = -\alpha L \tag{2.5}$$

Form equation 2.5
A represents absorbance of the material.
ε represents the molar absorptive of the material.
k represents the extinction coefficient of the light.
c represents the molar concentration of the material.
α represents the absorbance coefficient of the material.

2.8 Computed Tomography

Computed Tomography (CT), also called Computed Axial Tomography (CAT), is the most widely used imaging technology in radiology departments. The principle of the conventional or analog geometric tomography method is illustrated in Fig. 2.4. During image acquisition, the x-ray beam is moved linearly in one direction, while the x-ray film, which acts as the detector of the x-ray beam projected, is synchronously moved in the opposite direction [6], this displacement is linear and is repeated for different projection angles γ. Depending on the specific attenuation properties of the tissue, the intensity of the x-ray is attenuated on its path through the object. It is necessary to irradiate the object to be examined from all all directions, in order to, determine the spatial distribution inside a three dimensional object.

The amount of x-ray attenuation is measured by the detector and subsequently digitally recorded. For each angle γ, this yields to a simple one-dimensional radiography. From this initial radiography, it is still not possible to determine the spatial distribution of the tissue attenuation coefficients.To determine the spatial distribution of one slice, the objects need to be view sideways, since the projection angle is varied from 0° to 180°. Figure 2.5 shows the functionality for one angel γ.

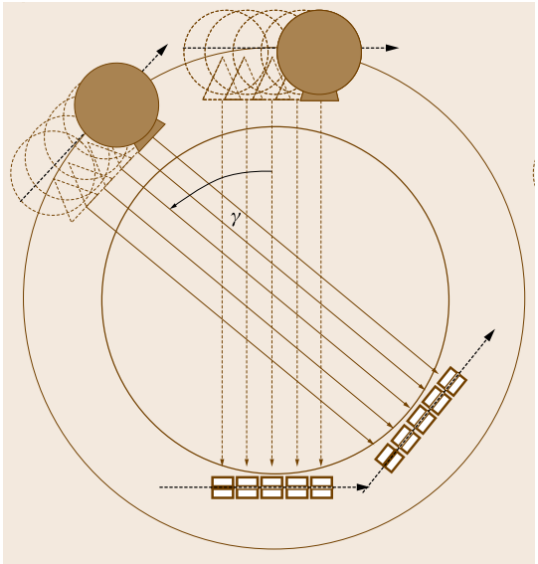

Figure 2.4: First generation of CT devices, equipped with a beam emitter and a single receptor. This are moved linearly, and the configuration is rotated through different projection angles γ [6].

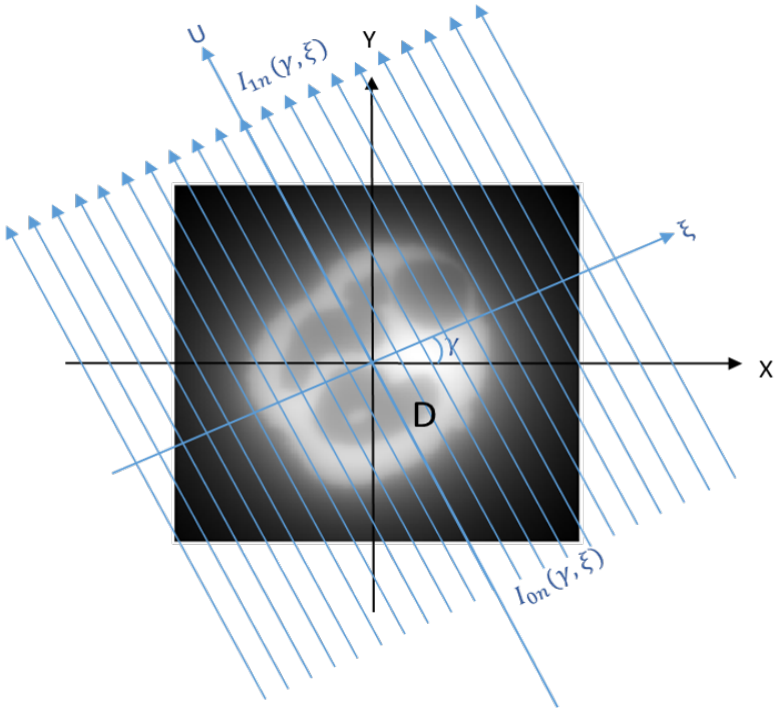

Figure 2.5: X-ray attenuation for one angle γ

2.8.1 Radon Transform

The Radon transform $Rf(x,y)$ is the projection of an object to the point in the plane the function $f(x,y) \in \mathbb{R}^2$ associates a scalar that generates a parallel projection in the direction of L as shown in figure 2.6, it is characterized by the line integrals of all the straight lines perpendiculars to the straight line ξ, that cross the origin and goes in direction of L, and is denoted by equation 2.6 [47]. The radon transform of a 2D image for angles 0 and 90, can be seen in figure 2.8 c) and d).

$$Rf(x,y) = \int_L f(x,y)du \tag{2.6}$$

As seen in figure 2.6 , the parametrization of the Radon transform equation 2.6, with values of x as shown in equation 2.7 and y as shown in equation 2.8.

$$x = \xi cos\gamma - usen\gamma \tag{2.7}$$

$$y = \xi sin\gamma + ucos\gamma \tag{2.8}$$

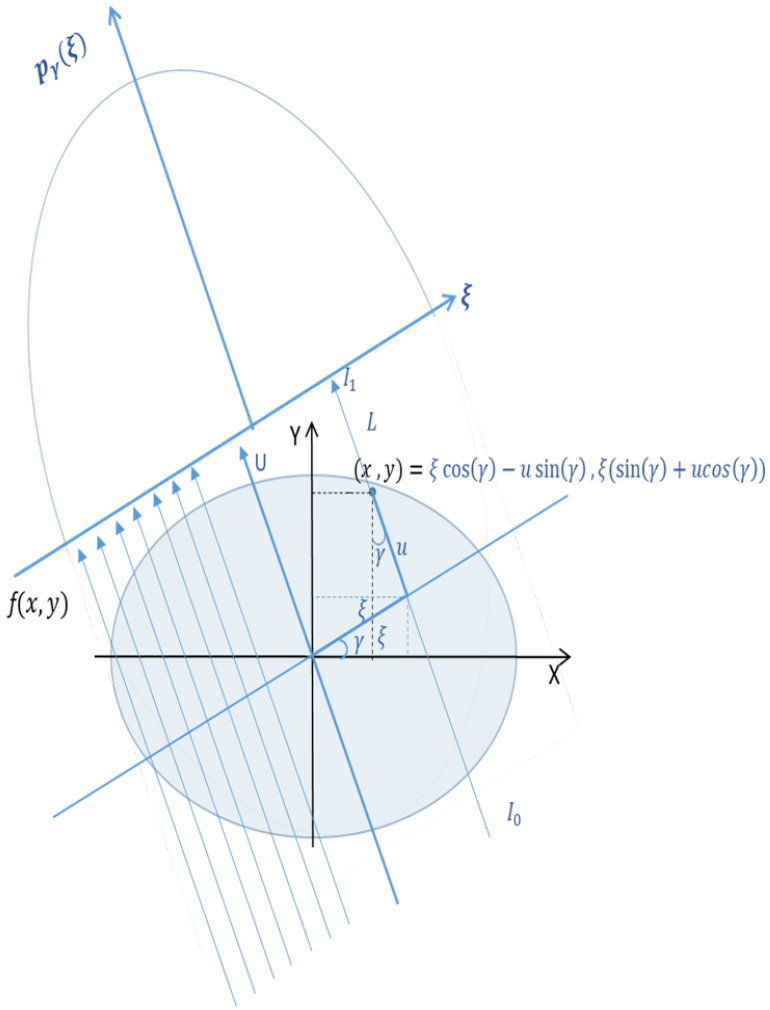

Figure 2.6: Parametrization for Radon Transform.

Then:

$$Rf(x,y) = p(\xi) = \int_L f(x,y)du \tag{2.9}$$

Parametrized Radon transform shown in equation 2.10:

$$p_\gamma(\xi) = \int_{-\infty}^{\infty} f(\xi cos\gamma - usen\gamma, \xi sin\gamma + ucos\gamma)du \tag{2.10}$$

The Radon transform has the next properties:

1. The projections are periodic and symmetric, with a period of 2π, $p_\gamma(\xi) = p_{\gamma+\pi}(-\xi) = p_{\gamma+2\pi}(\xi)$.
2. It's closely related to the one and two dimensions Fourier transform.
3. The domain of the data of the Radon transform generates a sinogram.

2.8.2 Sinogram

The sinogram is the graphic representation in a rectangular image of the set of data obtained from the Radon transform, in a way that each column of pixels represents a projection in light intensity levels. It gets the name of sinogram because looks like a set of multiples sines with different amplitudes and phases [48], as shown in figure 2.7.

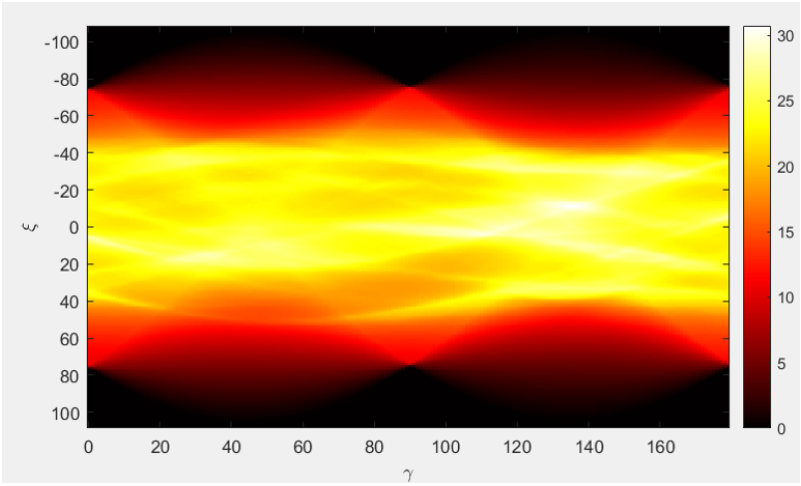

Figure 2.7: Sinogram.

In the sinogram every point of the image $f(x,y)$ is mapped for each of the directions of the beams or projections of that direction in a point that correspond the angle γ and the

distance from the center to the point ξ with an intensity u inside the domain of the projections obtained with the Radon transform.

A closer point to the center of the image will have a sinusoidal very short, close to a straight line, on the other side, if the selected point is located far away from the center of the image, will have a sinusoidal with a big amplitude. Any point of the image represented in polar coordinates can be represented in the sinogram.

2.8.3 Inverse Radon Theorem

Given $f(x,y)$ is possible to find the Radon transform. To solve the inverse problem, to find $f(x,y)$ starting from the Radon transforms $p_\gamma(\xi)$, Radon showed that is possible to recover a two variable function, using the Fourier transform and its inverse, when is known all the line integrals, meaning that, it is possible to reconstruct the image of an object if the data of each line that crossed the object is known [49]. Overlapping its projections $p_\gamma(\xi)$. The inverse radon transform of a 2D image for γ 0 and 90, can be seen in figure 2.8 e) and f).

2.8.4 Reconstruction of the Image

From a mathematical point of view, image reconstruction in computed tomography is the task of computing the spatial structure of an object. There are different techniques to reconstruct an image, nowadays the filtered backprojection is the most popular because has demonstrated to be the one with the better quality reconstruction [6].

The more projections for angles γ are collected, more accuracy the image can be reconstructed, as shown in 2.9.

Relation between the Fourier transform and the Radon transform is shown in equation 2.11.

Being $\mathscr{F}f(u,v)$ the Fourier transform of the function $f(x,y)$.

$$\mathscr{F}f(u,v) = \mathscr{F}(u,v) = \int_{-\infty}^{\infty}\int_{-\infty}^{\infty} f(x,y)e^{-j2\pi(ux+vy)}dxdy \tag{2.11}$$

The Fourier transform of the projection

$$\mathscr{F}p_\gamma(\omega) = P_\gamma(\omega) = \int_{-\infty}^{\infty} p_\gamma(\xi)e^{-j2\pi\omega\xi}d\xi \tag{2.12}$$

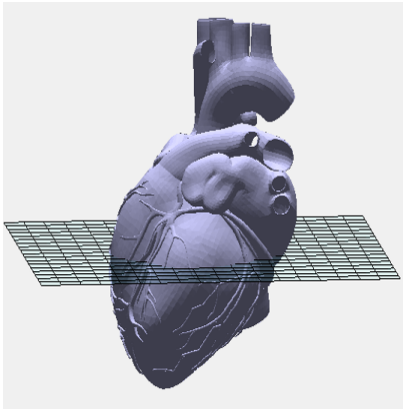

(a) Heart STL model with selected z-slice.

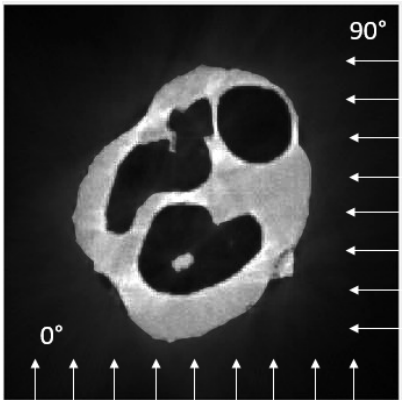

(b) Selected z-slice, top view.

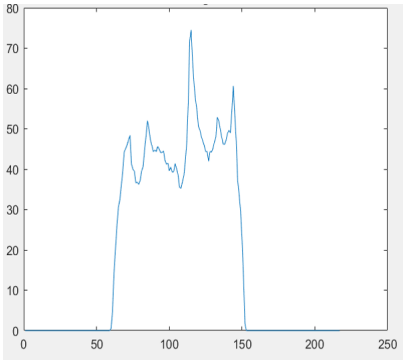

(c) Radon transform for $p_0(\xi)$.

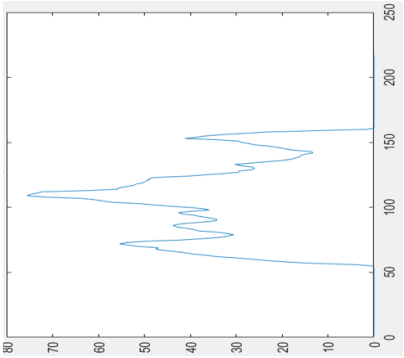

(d) Radon transform for $p_{90}(\xi)$.

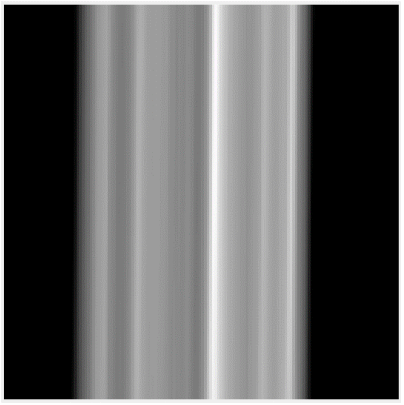

(e) Inverse Radon transform for $p_0(\xi)$.

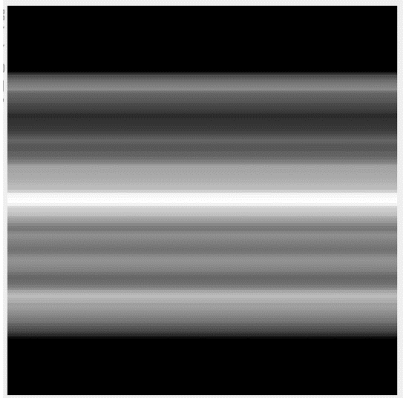

(f) Inverse Radon transform for $p_{90}(\xi)$.

Figure 2.8: Radon transform and Inverse Radon transform for 0 and 90 degrees of one z-slice.

$$\mathscr{F}p_\gamma(\omega) = \int_{-\infty}^{\infty}\int_{-\infty}^{\infty} f(\xi cos\gamma - usen\gamma, \xi sin\gamma + ucos\gamma)e^{-j2\pi\omega\xi}dud\xi \tag{2.13}$$

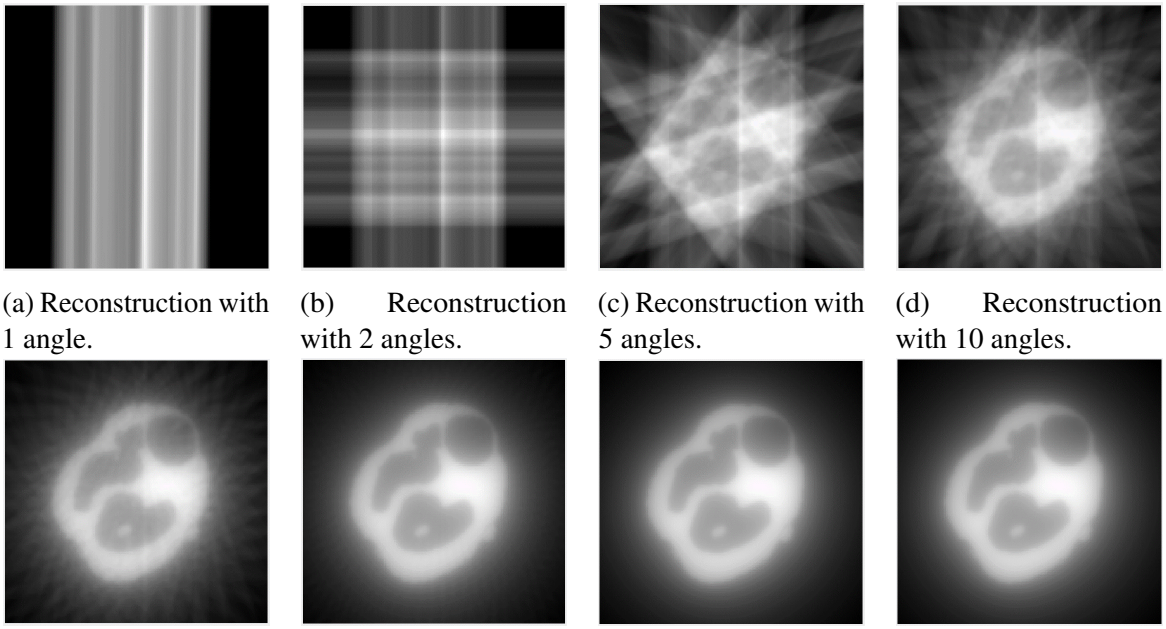

(a) Reconstruction with 1 angle. (b) Reconstruction with 2 angles. (c) Reconstruction with 5 angles. (d) Reconstruction with 10 angles.

(e) Reconstruction with 20 angles. (f) Reconstruction with 45 angles. (g) Reconstruction with 90 angles. (h) Reconstruction with 180 angles.

Figure 2.9: Image reconstruction.

Given that

$$x = \xi cos\gamma - usen\gamma \tag{2.14}$$

$$y = \xi sin\gamma + ucos\gamma \tag{2.15}$$

With a Jacobian of one.

$$\mathscr{F} p_\gamma(\omega) = \int_{-\infty}^{\infty}\int_{-\infty}^{\infty} f(x,y)e^{-j2\pi(xcos\gamma+ysin\gamma)}dxdy \tag{2.16}$$

$$\mathscr{F} p_\gamma(\omega) = \mathscr{F} f(\omega cos\gamma, \omega sin\gamma) \tag{2.17}$$

$$P_\gamma(\omega) = F(\omega cos\gamma, \omega sin\gamma) \tag{2.18}$$

This equation represents the Fourier slice theorem. The Fourier transform of the projections give us the values of the Fourier transform of $f(u,v)$ along the line that form an angle γ with the x-axis.

The main problem that can be found with the Fourier slice theorem is for high frequencies, where the points can be found far apart from each other, this implies that an interpolation is required, which can produce a significance error. A way to solve this problem, is filtering the frequency domain before getting the Inverse Fourier transforms to get the projections, this is known as filtered backprojection.

2.8.5 Fourier Filter Backprojection

Bi-dimensional inverse Fourier transform

$$f(x,y) = \int_{-\infty}^{\infty}\int_{-\infty}^{\infty} \mathscr{F}(u,v)e^{j2\pi(ux+vy)}dudv \tag{2.19}$$

Substitute $u = \omega cos\gamma$ and $v = \omega sin\gamma$, with ω Jacobian.

$$f(x,y) = \int_{0}^{2\pi}\int_{0}^{\infty} \omega\mathscr{F}(\omega cos\gamma, \omega sin\gamma)e^{j2\pi(xcos\gamma+ysin\gamma)}d\omega d\gamma \tag{2.20}$$

$$f(x,y) = \int_{0}^{\pi}\int_{-\infty}^{\infty} ||\omega||\mathscr{F}(\omega cos\gamma, \omega sin\gamma)e^{j2\pi(xcos\gamma+ysin\gamma}d\omega d\gamma \tag{2.21}$$

$$f(x,y) = \int_{0}^{\pi}\int_{-\infty}^{\infty} ||\omega||P_{\gamma}(\omega)e^{j2\pi(xcos\gamma+ysin\gamma)}d\omega d\gamma \tag{2.22}$$

This equation is known as Fourier Filter Backprojection [50]. Where the first integral represents the filter to the projections $p_{\gamma}(t)$ to generate filtered projections $p_{\gamma}^{\omega}(t)$.

$$p_{\gamma}^{\omega}(t) = \int_{-\infty}^{\infty} ||\omega||P_{\gamma}(\omega)e^{j2\pi(xcos\gamma+ysin\gamma)}d\omega \tag{2.23}$$

$$p_{\gamma}^{\omega}(t) = \int_{-\infty}^{\infty} ||\omega||P_{\gamma}(\omega)e^{j2\pi\omega}d\omega \tag{2.24}$$

By last, it is necessary to calculate the second integral of the Fourier filtered backprojection to obtain $f(x,y)$

$$f(x,y) = \int_0^{\pi} p_{\gamma}^{\omega}(xcos\gamma, ysin\gamma)d\gamma \tag{2.25}$$

2.9 Computed Axial Litography

Computed Axial Litography (CAL) printing also known as volumetric printing, is a technique capable of reconstruct structures based on the tomography concept and the Beer-Lambert law, this permits the creation of geometrically complex, millimeter-scale constructs at an unprecedented printing velocity, opening new avenues for upscaling the production of hydrogel-based constructs and for their applications on tissue-engineering, regenerative medicine, and soft robotics [9], the method consists of projecting a rotating photocuring resin from all angles, in a way that, a complete volume is reconstructed simultaneously, the CAL concept can be seen in figure 2.10.

The CAL printing technique applied to the medial industry has the potential to revolutionize the area of organs transplants, regenerative medicine and more areas related with the bioprinting industry.

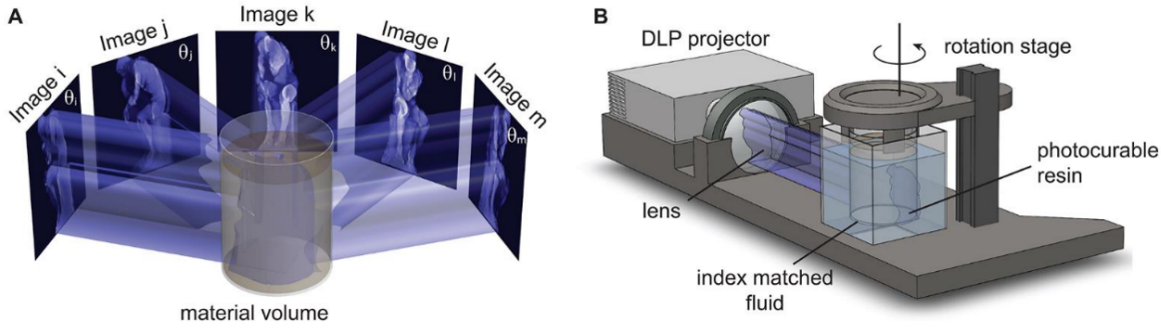

Figure 2.10: CAL printing technique used in [7]. A) Volumetric reconstruction concept. B) Mechanical System.

Chapter 3

Design and Methodology

3.1 Mechanical System

The mechanical system, represented in 3.1 and 3.2, consists of a standard projector, a lens, needed to focus the light, a stepper motor that acts as a rotation stage, a vial where the hydrogel is contained, and an external container.

The projector used for this project was a standard projector QKK AK-80, with a brightness of 2200 lumens, a native resolution of 800x480 pixels, and a contrast ratio off 2000:1. The lens used in the experiments is a biconvex lens with a focal distance of 75mm and a diameter of 25mm, assembled with a neutral filter, it can be seen in 3.3, most tomography algorithms supposed a perfectly straight beam of light, but in practice every light beam has a certain divergence [51]. To create the rotation of the vial, an stepper motor was used, for most experiments the rotation was a constant 15° per second. An external container was proposed to be used to contained a matched reflection index fluid, but was not necessary for the experiments, and instead used sometimes to keep the hydrogel at low temperatures.

3.2 Material Characterization: Absorbance and Penetration Depth

In order to select the correct wavelength and material needed to be used, an absorbance test was performed of the possible materials to be selected. The selected material and wavelength should have enough absorbance that the material could be crosslinked with visible light, but

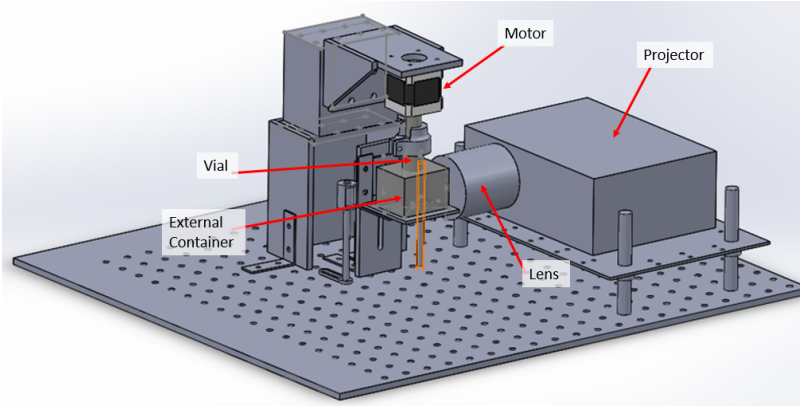

Figure 3.1: Design of the mechanical system.

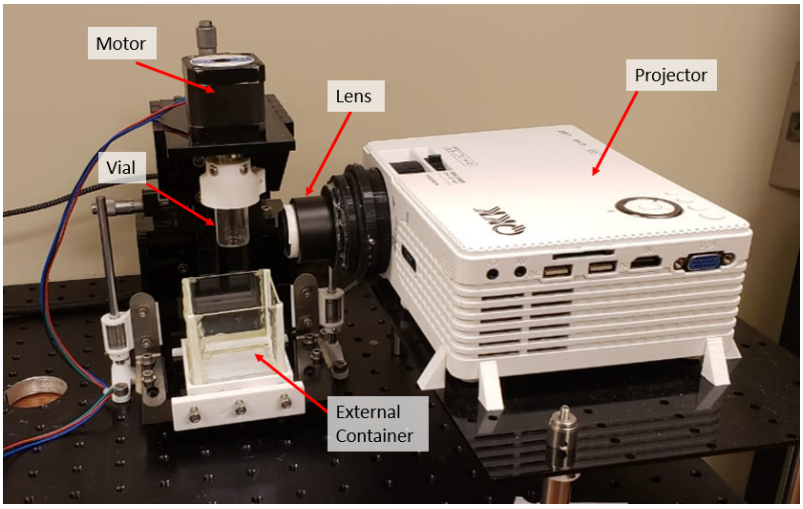

Figure 3.2: Implementation of the mechanical system.

Figure 3.3: Lens used in the projector, assembled with a neutral filter.

RU mM	0.25	0.5	0.75	1.0	1.25	1.5
GelMA 10%	A1/A2	B1/B2	C1/C2	D1/D2	E1/E2	F1/F2

Table 3.1: Concentrations of RU for 10% GelMA, absorbance test shown in figure 3.4.

also is important to have enough penetration depth to reach without complications the radius of the vial that were used [51], in this case the vial diameter is 1.2 cm.

Light which is transferred through a semiconductor material is reduced by a substantial amount when it passes through. The absorbance, which is the absorption of light rate is directly proportional to the light intensity, known as photon flux, for a specific wavelength [52], as light passes through the material the photon flux reduced because on the way through some photons are absorbed. So, the amount of photons that would reach a specific point in a semiconductor depends on both the photon wavelength and the distance from the surface. Penetration depth is a measure of how deep light can penetrate into a material. It is defined as the depth at which intensity of the radiation inside the material falls $1/e$ (about 37%) of its value just beneath the surface [53].

An absorbance test was performed in a plate reader Infinite 200Pro, using the application Tecan i-control, selecting wavelengths from 400nm to 600nm, with a wavelength step size of 5nm, and utilizing 25 flashes per wavelength, to measure the absorbance of GelMA 10% and different concentrations of RU as photoinitiator. The material for the test was GelMA with different concentrations of photoinitiator of RU-SPS. The samples were GelMA with concentrations of 0.25 mM RU, 0.5 nM RU, 0.75 mM RU, 1 mM RU, 1.25 mM RU and 1.5 mM RU, as shown in table 3.1 and figure 3.4, the test was performed for all the 12 samples of 100 μl each.

If we know that the penetration depth DP is given by 1 divided by the absorbance coefficient, as shown in equation 3.1 and that the absorbance coefficient is given by equation 3.2, where A represents the absorbance, and t the thickness.

$$DP = 1/\alpha \tag{3.1}$$

$$\alpha = ln(10) * (A/t) \tag{3.2}$$

From equation 3.2 the absorption coefficient can be calculated, given that the thickness used was 0.1334 cm, and using the absorbance from the test. With the absorption coefficient, the penetration depth can be calculate. The results from the penetration depth calculation can

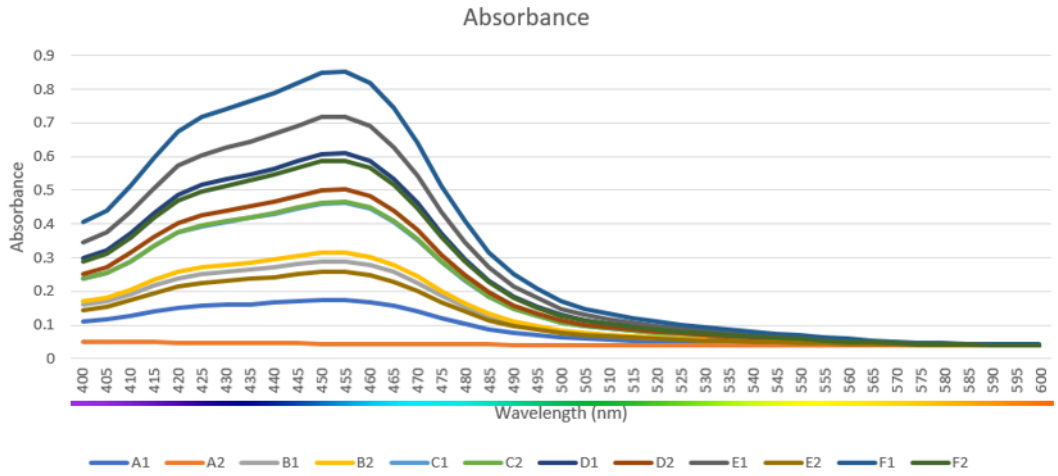

Figure 3.4: Absorbance test for concentrations of table 3.1.

be shown in figure 3.5, where A2 (orange line) suffered from an air bubble, causing it to be rejected from this test.

The penetration depth of the wavelength used has a lot of importance in this experiment, it has to be enough to crosslink the material and to cover the radius for the vial used, in this case the radius vial was of 0.6 cm. Analyzing the penetration depth of the different wavelength for the different concentrations of materials, from the figure 3.5 and table 3.2, it can be seen that using the green channel (520nm) the radius of the vial can be covered, for the GelMA experiments the green channel was selected to be used with an RU concentration of 1mM and 1.5mM.

3.3 Crosslinking of the Material

Multiple calibration tests were performed in order to achieve the best results, the focus of the projector was center in the center of the vial, the light intensity needed to photocrosslink the material.

Crossinking of the Material

The material selected, 10% GelMA with 1mM RU and 1.5mM RU, were projected with different light wavelengths in a SLA printer, for a couple of minutes, this was made with the purpose to prove crosslinking of the material, not caring about the time of crosslinking, given that, those concentrations of material have a good penetration depth with the green channel.

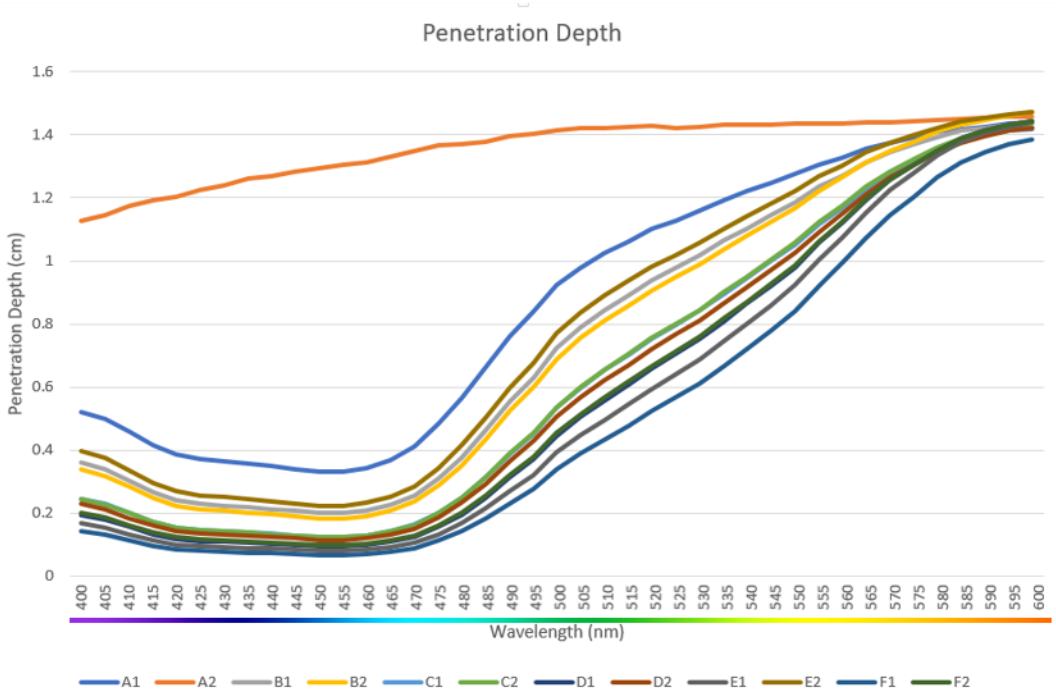

Figure 3.5: Penetration depth in cm for concentrations of table 3.1.

As it can be seen from 3.6, even if the crosslinking was achieved with both concentrations, the GelMA concentration with 1.5mM RU had a better result in the crosslinking test.

The material used in this project is gelatin methacryloyl (GelMA) polymer. The photoinitiator used was a two-part visible light initiator consisting of tris(2,2-bipyridyl)dichlororuthenium(ll) hexahydrate (RU) and sodium persulfate (SPS). RU and SPS were mixed at concentrations of 1mM and 10mM respectevely into GelMA hydrogel.

Hydrogels samples were cooled down in a refrigerator to temperatures between 2° and 5° to induce reversible thermal gelation and render the samples solid before photocrosslinking.

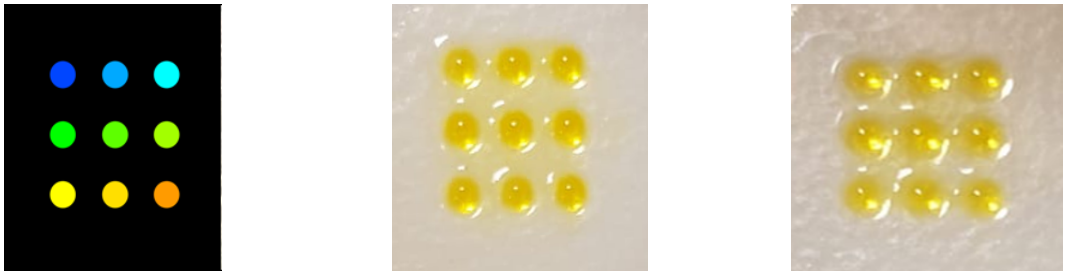

(a) Projected image. (b) GelMA and 1mM RU. (c) GelMA and 1.5mM RU.

Figure 3.6: Crosslinking test for GelMA.

Wavelength 520nm			
RU Concentration (mM)	Absorbance	Absorption coeff. (α)	Penetration Depth (cm)
0.25	0.0526	0.9083	1.1009
0.25	0.0405	0.6993	1.4298
0.5	0.0616	1.0637	0.9400
0.5	0.0639	1.1034	0.9062
0.75	0.0769	1.3279	0.7530
0.75	0.0767	1.3244	0.7550
1.0	0.0880	1.5196	0.6580
1.0	0.0803	1.3866	0.7211
1.25	0.0975	1.6836	0.5939
1.25	0.0589	1.0171	0.9831
1.5	0.1106	1.9098	0.5235
1.5	0.0868	1.4989	0.6671

Table 3.2: Absorbance, absorption coefficient and penetration depth for GelMA with different concentration of RU.

This was made to make sure that the material stays in the same position, and there is no kinetic force inside the material during the photocrosslinking, once the material is photocrosslinked, the thermal gelation is reverse in order to separate the GelMA sections crosslinked with the ones that didn't crosslinked.

3.4 Software

Based on a software code for tomography reconstruction [7], and on the theory explain in Chapter 2 about Computed Tomography and image reconstruction, a Matlab code was implemented in order to obtain the corresponding projections for angles θ from 0° to 180°, when the target gets projected from all angles with the respective projection, and the light dose is enough to crosslinked the material, then the volumetric printing is completed.

For an example a heart model is presented where in figure 3.7 can be seen the heart model with a slice in the z-axis selected and the respective dose slice, for different slices of the model, the dose slice calculation is based on the principle described in chapter 2, the dose slice is calculated for all the different slices of the model for the z-axis.

Once the dose slice is calculated for the complete model, the summation of the slices is arranged in a way that is able to calculate the different projections for all angles with the corresponding slice, the optimized projection can be seen in figure 3.8.

With the optimized projections for angles θ 0° to 180°, the projections are ready to being transmitted to the projection system, for this case, as mention in the previous section the wavelength selected is 520 nm (the green channel), the actual projections from the projection system can be observed in figure 3.9 for θ 0°, 60°, 120° and 180°.

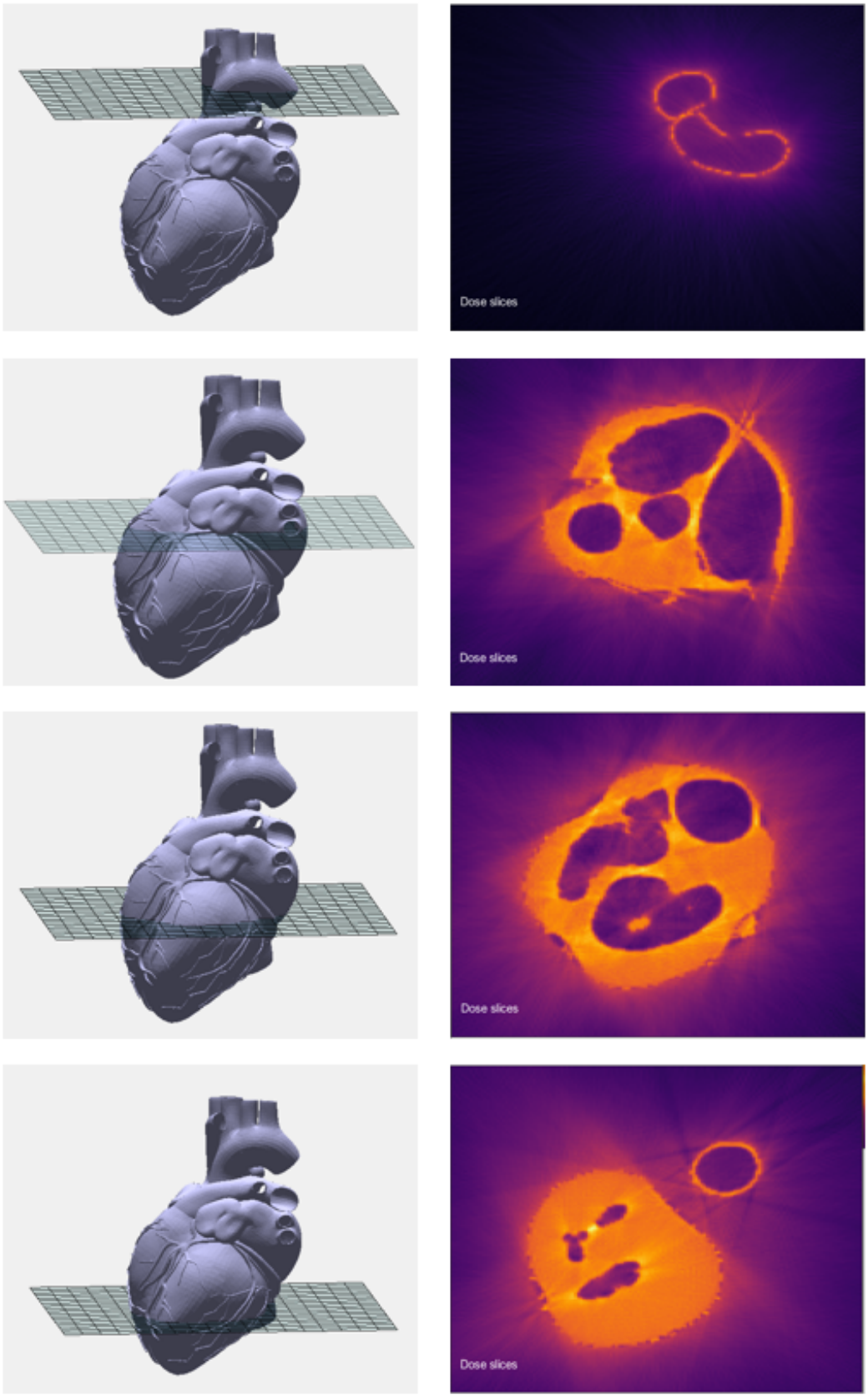

Figure 3.7: Dose slice for different slices in z-plane. Left STL model with the slice selected. Right, dose calculated for the selected slice.

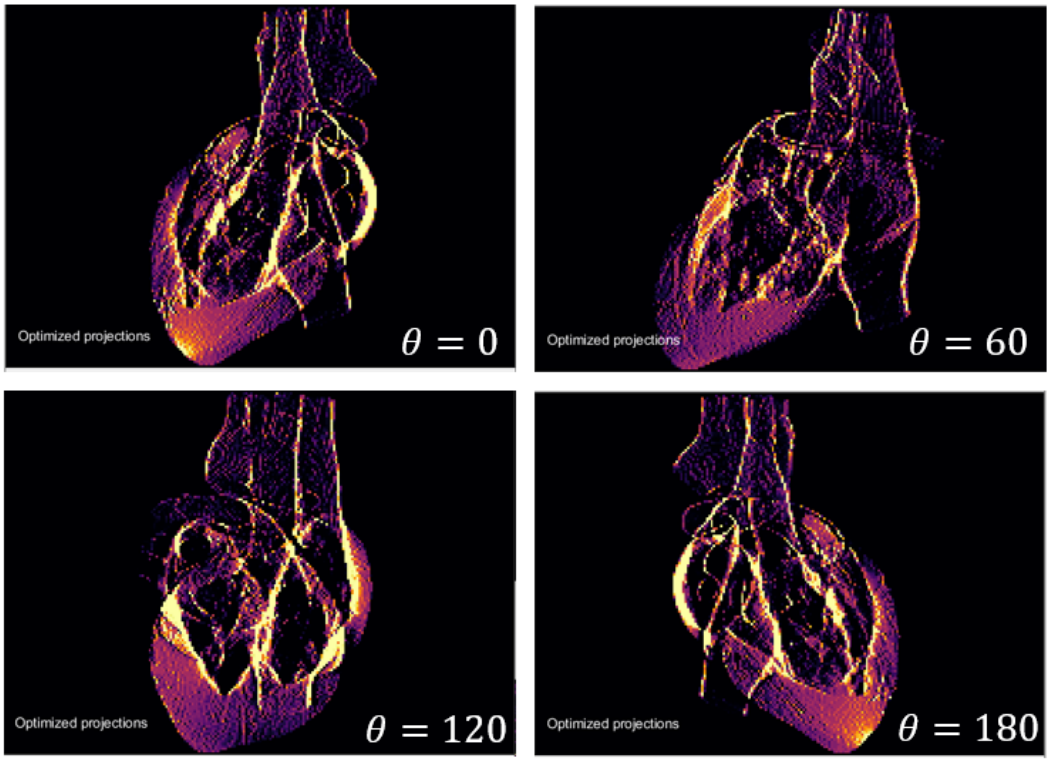

Figure 3.8: Optimized projections for $\theta = 0, 60, 120, 180$.

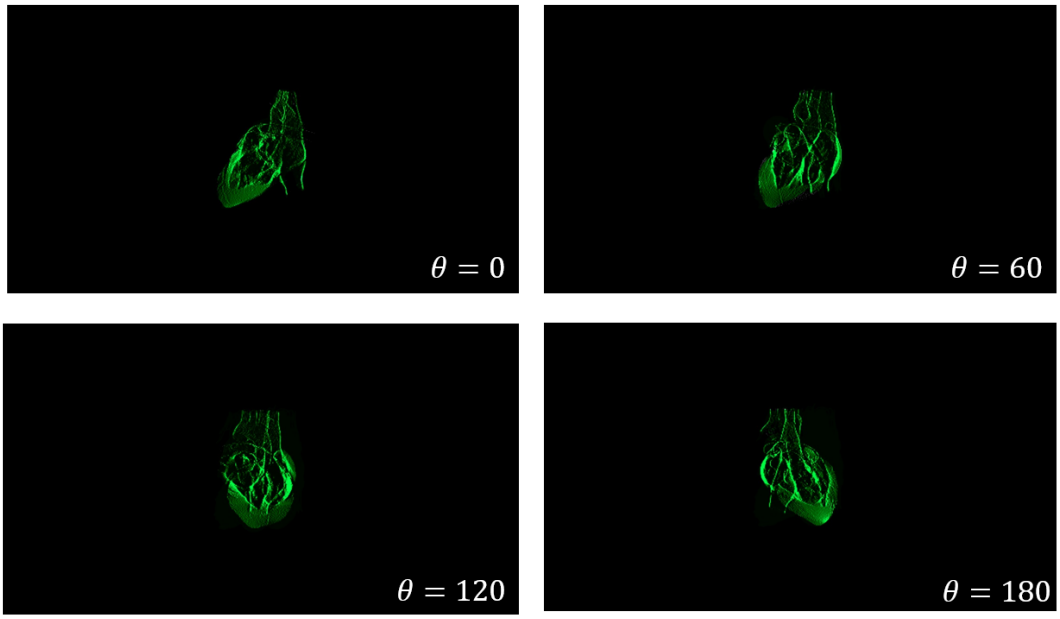

Figure 3.9: Real projections for $\theta = 0, 60, 120, 180$.

Chapter 4

Results

Several tests were performed in order to 3D print different geometries using GelMa as hydrogel and RU as photoinitiator. Both solid and shapes with hollows were successfully achieved, some of the printed shapes, and the description of the experiment, are shown in this section.

4.1 Solid shapes

The first printed shape, considered the easiest was a solid sphere, as discussed in chapter 3, the material selected was GelMa with 1mM RU, using the 520nm wavelength (green colour). The printing process is describe briefly in this section, being similar printing process for all the printing shapes. First, once the material is ready and poured in the vial, the temperature of the material is low down between -4°C and 10°C, which is the temperature where the material behaves in solid state [**?**], this is made with two purposes, to make sure the material stays in the same place while rotating, preventing to generate air bubbles or misaligned with the projections, and to make sure the cross linked sections of the material conserves the same density and doesn't sink to the bottom of the vial, this is a great advantages of working with this material in comparison with others commonly used where the material remains in a liquid state the hole process. Once the material is ready is placed in the rotation stage, which starts rotating at constant 15° per second, then, the projections synchronized with the rotation stage at 15 frames per second start projecting the respective frame for each angle, an example of how the frames of the projections looked can be seen in figure 4.1, the projections continues until the 3D shape its completely formed, the printing process can be seen in figure 4.2, the material target starts cross linking the complete volume simultaneously as it rotates,

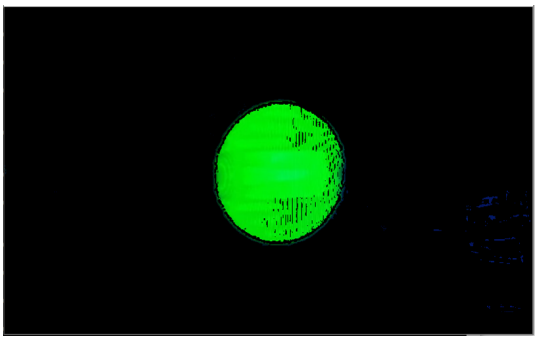

Figure 4.1: Frame projected of green channel for sphere reconstruction.

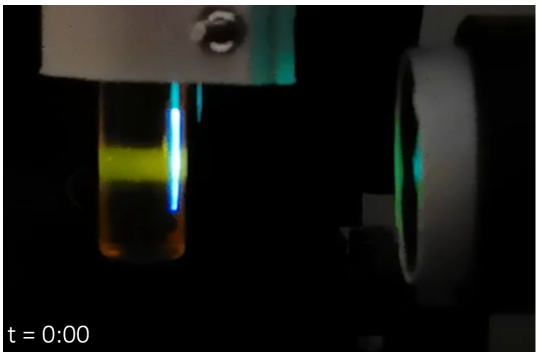

(a) Printing process of a sphere, printing time = 0 min.

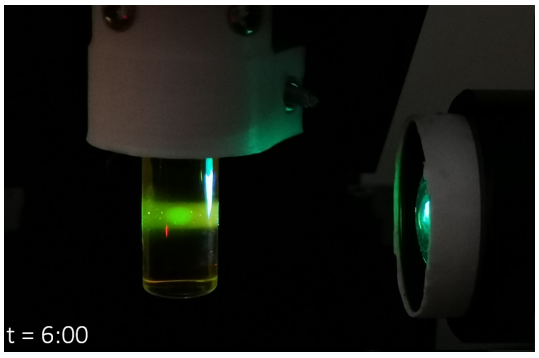

(b) Printing process of a sphere, printing time = 6 min.

Figure 4.2: 3D printing process of a sphere.

and not layer by layer as the common printing techniques, once its complete, the rotation stops and the vial is taken out for warming until the material becomes liquid again, then is separated the cross linked part of the material, which is the desired shape.

In figure 4.3 it can be seen the result from printing a sphere, the total printing time for this specific shape was 6:30 minutes, the expected diameter was 5mm, which is the resulted printed diameter.

The same procedure to achieve the printing of the sphere is applied to different figures, changing the projections according to the desired shape. Some of the solid shapes printed can be found in figure 4.4, the material used for all of the solid shapes printed, being all of them regular geometries, was GelMa with 1mM RU, the printing time, and the size of each of them can be found in table 4.1.

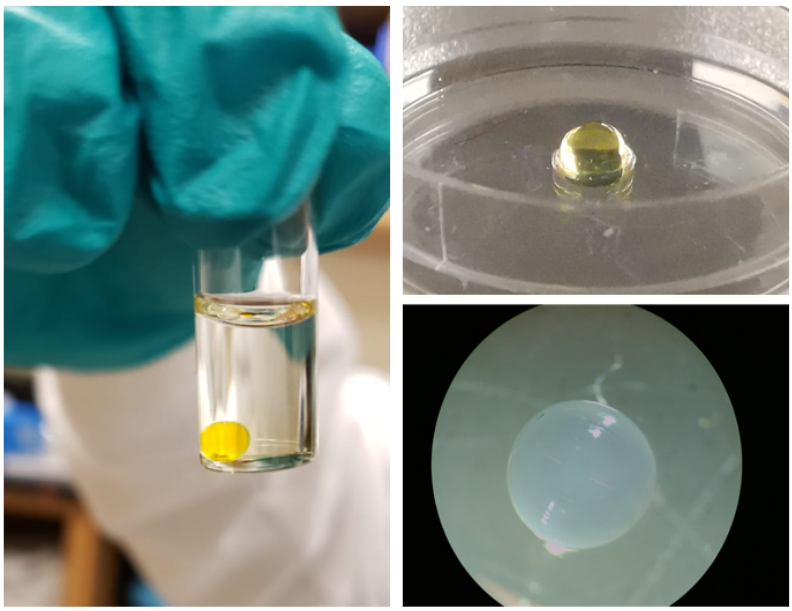

Figure 4.3: Printed sphere. Left, sphere resting in vial with water. Top, sphere resting in plate. Bottom, sphere under microscope (30x).

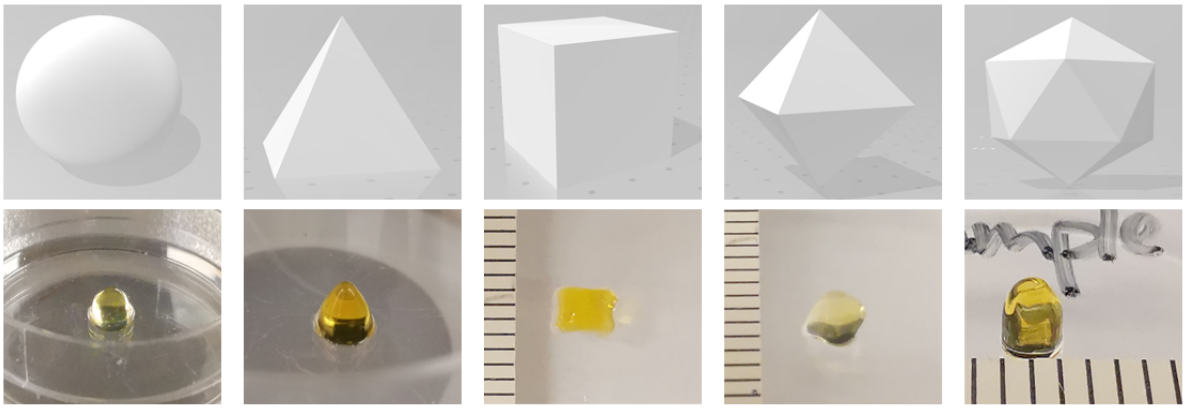

Figure 4.4: Printed solid shapes. Top, STL models. Bottom, printed shapes. Left to right geometries, sphere, square pyramid, cube, octahedron, icosahedron.

Shape	Height (mm)	Printing time (min)
Sphere	5.00	6:30
Square Pyramid	4.00	4:30
Cube	5.00	6:00
Octahedron	4.00	4:00
Icosahedron	5.00	7:00

Table 4.1: Height and printing time for solid shapes.

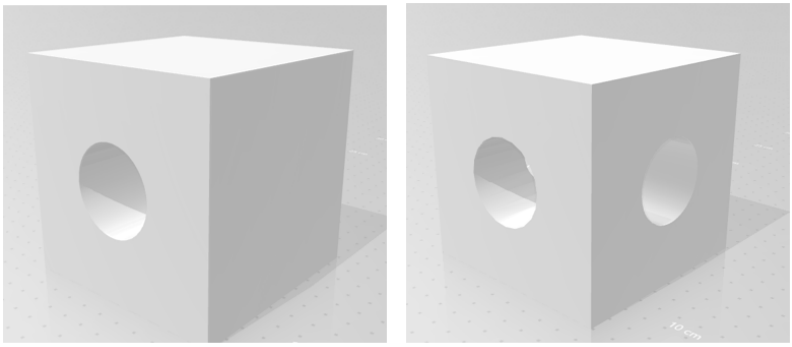

Figure 4.5: STL models. Left, cube with one hole. Right, cube with two cross holes.

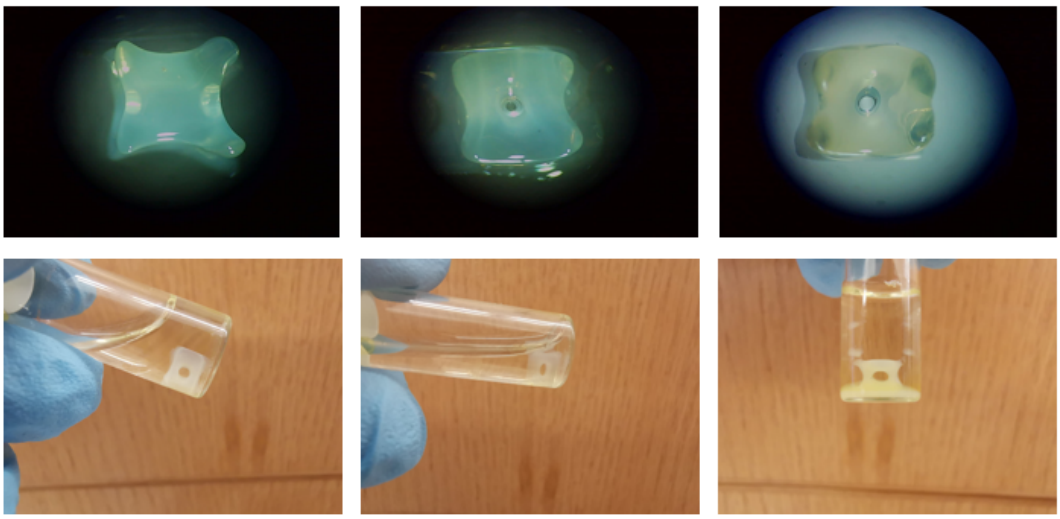

Figure 4.6: Printing result, cube with one hole.

4.2 Shapes with hollows

After successfully printing solid shapes, the next challenge was to 3D print shapes with hollows, for this part two geometries were proposed, a cube with a hollow that go through it, and a cube with two hollows that cross in the center of the cube, the STL model can be seen in figure 4.5.

The procedure for preparing the material and the printing process was similar to the one for the solid shapes, for the cube with one hole that can be seen in figure 4.6, the printing time was 7 min, the height of the hole figure is 5mm, and the hole diameter is 1mm, and for the cube with two holes, that can be seen in figure 4.7 the printing time was 6:30 min, the height of the hole figure is 5mm, and the hole diameter is approximately 1mm.

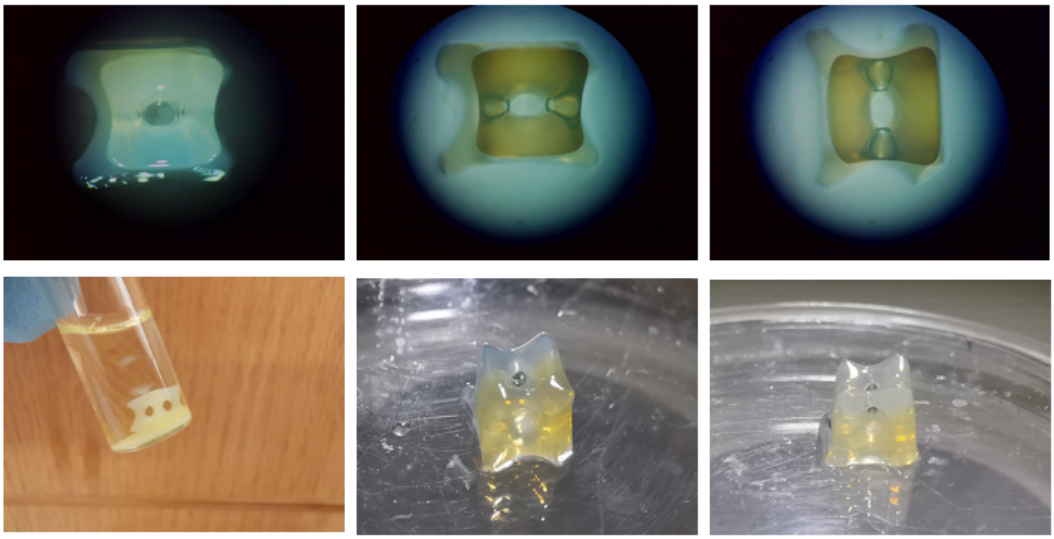

Figure 4.7: Printing result, cube with two cross holes.

Chapter 5

Discussion

In this chapter is presented discussion related from the previous chapters.

As it can be seen in chapter 4 Results, it was successfully 3D reconstructed solid geometries and geometries with hollows, however, there are certain aspects that can be improved in order to achieve better results.

The main goal of this project which is to achieve 3D printing using the CAL technique applied for biomaterials, in this particular case GelMa, and it was successfully reproduced, but the CAL technique can be improve by speeding up, scaling up, and increasing the resolution, these three specification can be achieved almost instantly by acquiring another set of lenses and a new projector with better native resolution, more brightness and highest contrast ratio.

As it can be seen from the previous chapter, in figure 4.4 the solid shapes were successfully printed, however, there can be observed some resolution problems in some of the figures. The sharp edges of some figures, like the cube and the square pyramid, it can be observed that the frame rate match the angular velocity of the rotation stage. For the sphere and the cube, it can be say that the printed is achieved as desired, but when the shape becomes more complex, like the octahedron and icosahedron, where the shape have more angles, the resolution is not enough, specially considering the small printed size.

For the printed shapes with hollows, that can be appreciated from figures 4.6 and 4.7, it is proved that it can be achieved holes that can last in GelMa with CAL techniques, this is very important achievement for the bioprinting, given the softness of the biomaterials, shapes with hollows may collapse, another important feature of these printed shapes is that holes and tubes are important geometries for a lot of biological structures, like veins and vessels [54].

As it can be seen from the printed shapes with holes, suffered from some deformation, this can be pointed out to the creation of the hollows and the softness of the material.

Once that the printed shape is complete, cell culturing is needed in order to be adequate for a biological guest, where the desired cell type depending on the application are needed to be grown in the printed figure as mentioned in chapter 2, but considering that GelMa has been proved to be a great material for cell culture [44], this should not represent a major problem.

Statistical tests based on computer vision can be applied to the printed results, as shown in [55], measuring the deformation grids comparing a perfect model with the result printed, it can be determined the best printed result and make adjustments to the printing technique in order to achieve better quality results.

CAL printing presents a lot of advantages over the conventional 3D printing techniques like the ones mentioned in Chapter 2 and in [16] where it can be seen a comparison made for printing speed and resolution, for the experiments made in this thesis, the printing speed is similar to the other approaches, but it should be more faster if the light intensity is increased, shortening the crosslinking time needed, another advantage that can be found from CAL printing, is that the material that is not crosslinked can be re-utilized if it properly store, it may need some processing technique.

It is truth that there are a lot of benefits from CAL 3D printing technique in comparison with the others 3D printing techniques, one big disadvantages from this printing technique is the printing size, to scale up the printed size it will be needed a great amount of material, that sometimes can be very difficult to acquire, also it will be needed a light intensity strong enough.

Chapter 6

Future Work

In this chapter future work to the hardware, software and applications of the implemented system is proposed.

6.1 Simultaneous Multi-material Reconstruction

One of the challenges for 3D printing nowadays is the use of multiple materials, specially if the printing of them is simultaneous.

Different tissues with different functions can be found in the human body, like epithelial tissue, nervous tissue, muscle tissue and connective tissue. Most of biological structures are made with multiple tissues, if it is wanted to replicated them with bioprinting techniques, then is needed to reconstructed the desired geometries with the application of multiple materials simultaneously.

In this concept, is proposed a simultaneous multi-material reconstruction, utilizing two different materials with a different photo-initiator each of them, in a way that each of the materials photo-react to start cross linking with a different wavelength.

The two different materials should be in the same vial mixed in a way that both of them are able to photo-react to a respective wavelength, then the STL model desired should be separated in two different models, each for a single material, an example of the voxel reconstruction it can be seen in figure 6.1, to illustrate this example a brain model is used and divided the voxel of the complete model into two different voxel matrices, for each hemisphere, the aim is that in the resulting printing figure the right hemisphere is made of one material that was crosslinked with a certain wavelength, and the left hemisphere a different

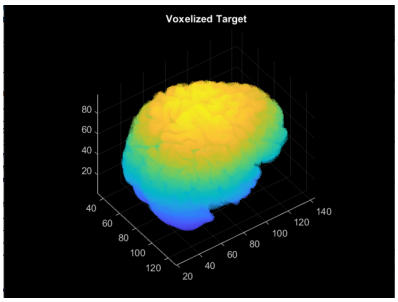

(a) Voxelized target, complete brain.

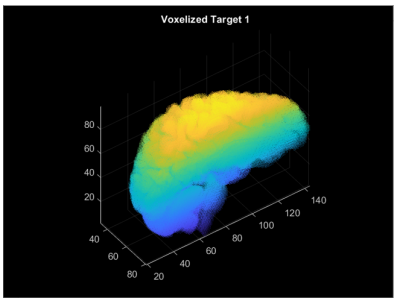

(b) Voxelized target 1, left hemisphere.

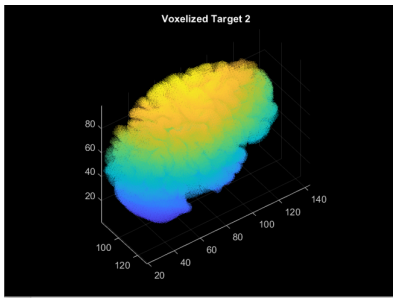

(c) Voxelized target 2, right hemisphere.

Figure 6.1: Voxelized targets for multi-material reconstruction.

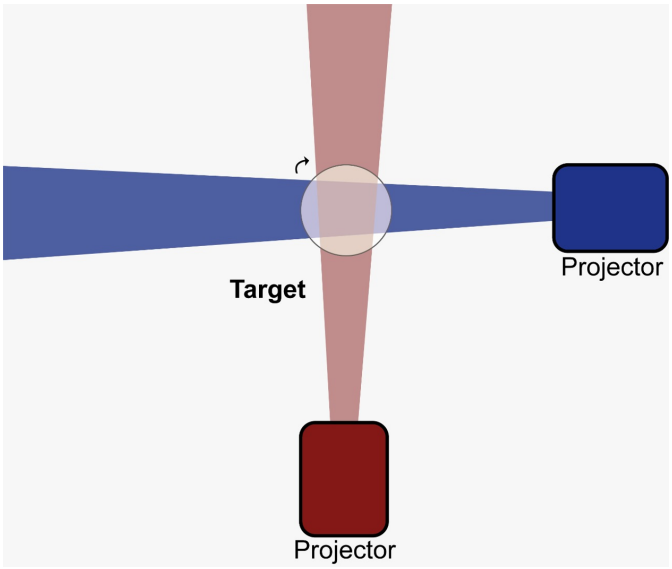

Figure 6.2: Proposed system for simultaneous multi-material CAL printing.

material than the right one and crosslinked with a different wavelength,it is important that the matrix size of each of the models match the original size matrix to be able to reconstruct the model.

For this example, a proposed mechanical system can be seen in figure 6.2, where two projectors are used, each with a different wavelength. The projections should be coordinated with the angular velocity of the rotation stage, and de-phased respecting the other one depending on the angle difference of the projectors with the vial. Figure 6.3 simulates the result of the simultaneous multi-material printing for a brain model, each colour represents a different material.

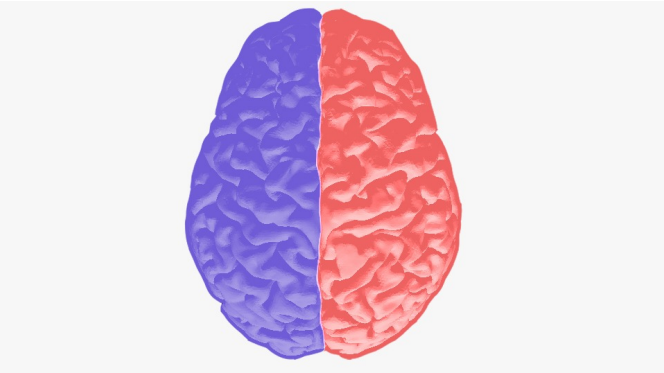

Figure 6.3: Simultaneous multi-material reconstruction printing result.

Chapter 7

Conclusion

In this thesis is demonstrated that applying the principle of the Computed Tomography, the viability of the Computed Axial Lithography (CAL) printing technique into the bioprinting area, which means, reconstructing a volume simultaneously from projecting a photo-curable resin (bioink), reconstructing 3D structures made of biomaterial, in this case GelMA, that has been proved to be capable of carried living cells.

Successful 3D shapes were printed using the CAL system implemented, solid shapes and shapes with hollows, proving that the technology can be applied to GelMA, some opportunities areas were found, like the resolution and the printing time that can be improved with a better projector.

CAL printing has been demonstrated to have advantages over conventional 3D printing techniques, printing speed, printing resolution, minimum waste of material, and more. CAL printing will be a great technique for the medical area, with limitless applications in tissue engineering and regenerative medicine.

The reproduction of the CAL printing system for biomaterials, in this particular case GelMA, is proved, opening the doors for applying the same concept to different biomaterials, which could have limitless applications in many distinct research areas.

Bibliography

[1] National Survey of Organ Donation Attitudes and Practices: Report of Findings. U.S. Department of Health and Human Services; 2019.

[2] Mandrycky C, Wang Z, Kim K, Kim DH. 3D bioprinting for engineering complex tissues. Biotechnology advances. 2016;34(4):422–434.

[3] Skardal A, Zhang J, Prestwich GD. Bioprinting vessel-like constructs using hyaluronan hydrogels crosslinked with tetrahedral polyethylene glycol tetracrylates. Biomaterials. 2010;31(24):6173–6181.

[4] Müller M, Öztürk E, Arlov Ø, Gatenholm P, Zenobi-Wong M. Alginate sulfate–nanocellulose bioinks for cartilage bioprinting applications. Annals of biomedical engineering. 2017;45(1):210–223.

[5] Knowlton S, Tasoglu S. A bioprinted liver-on-a-chip for drug screening applications. Trends in biotechnology. 2016;34(9):681–682.

[6] Buzug TM. Computed tomography. In: Springer Handbook of Medical Technology. Springer; 2011. p. 311–342.

[7] Kelly BE, Bhattacharya I, Heidari H, Shusteff M, Spadaccini CM, Taylor HK. Volumetric additive manufacturing via tomographic reconstruction. Science. 2019;363(6431):1075–1079.

[8] Ozbolat IT, Yu Y. Bioprinting toward organ fabrication: challenges and future trends. IEEE Transactions on Biomedical Engineering. 2013;60(3):691–699.

[9] Bernal PN, Delrot P, Loterie D, Li Y, Malda J, Moser C, et al. Volumetric Bioprinting of Complex Living-Tissue Constructs within Seconds. Advanced materials. 2019;31(42):1904209.

[10] Gibson I, Rosen DW, Stucker B, et al. Additive manufacturing technologies. vol. 17. Springer; 2014.

[11] Bandyopadhyay A, Bose S. Additive manufacturing. CRC press; 2019.

[12] Lavik E, Langer R. Tissue engineering: current state and perspectives. Applied microbiology and biotechnology. 2004;65(1):1–8.

[13] Lanza R, Langer R, Vacanti JP, Atala A. Principles of tissue engineering. Academic press; 2020.

[14] Langer R. Perspectives and challenges in tissue engineering and regenerative medicine. Advanced materials. 2009;21(32-33):3235–3236.

[15] Bartlett S. Printing organs on demand. The Lancet Respiratory Medicine. 2013;1(9):684.

[16] Murphy SV, Atala A. 3D bioprinting of tissues and organs. Nature biotechnology. 2014;32(8):773.

[17] Li J, Chen M, Fan X, Zhou H. Recent advances in bioprinting techniques: approaches, applications and future prospects. Journal of translational medicine. 2016;14(1):271.

[18] Tuan RS, Boland G, Tuli R. Adult mesenchymal stem cells and cell-based tissue engineering. Arthritis Res Ther. 2002;5(1):32.

[19] Guillotin B, Souquet A, Catros S, Duocastella M, Pippenger B, Bellance S, et al. Laser assisted bioprinting of engineered tissue with high cell density and microscale organization. Biomaterials. 2010;31(28):7250–7256.

[20] Pepper ME, Seshadri V, Burg TC, Burg KJ, Groff RE. Characterizing the effects of cell settling on bioprinter output. Biofabrication. 2012;4(1):011001.

[21] Duocastella M, Colina M, Fernández-Pradas J, Serra P, Morenza J. Study of the laser-induced forward transfer of liquids for laser bioprinting. Applied surface science. 2007;253(19):7855–7859.

[22] Gauvin R, Chen YC, Lee JW, Soman P, Zorlutuna P, Nichol JW, et al. Microfabrication of complex porous tissue engineering scaffolds using 3D projection stereolithography. Biomaterials. 2012;33(15):3824–3834.

[23] Nerem RM, Seliktar D. Vascular tissue engineering. Annual review of biomedical engineering. 2001;3(1):225–243.

[24] Zadpoor AA, Malda J. Additive manufacturing of biomaterials, tissues, and organs. Springer; 2017.

[25] Bose S, Vahabzadeh S, Bandyopadhyay A. Bone tissue engineering using 3D printing. Materials today. 2013;16(12):496–504.

[26] Pati F, Song TH, Rijal G, Jang J, Kim SW, Cho DW. Ornamenting 3D printed scaffolds with cell-laid extracellular matrix for bone tissue regeneration. Biomaterials. 2015;37:230–241.

[27] Chang R, Emami K, Wu H, Sun W. Biofabrication of a three-dimensional liver microorgan as an in vitro drug metabolism model. Biofabrication. 2010;2(4):045004.

[28] Wang Z, Samanipour R, Koo Ki, Kim K. Organ-on-a-chip platforms for drug delivery and cell characterization: A review. Sens Mater. 2015;27(6):487–506.

[29] Jhon MS, Andrade JD. Water and hydrogels. Journal of biomedical materials research. 1973;7(6):509–522.

[30] Nair LS, Laurencin CT. Polymers as biomaterials for tissue engineering and controlled drug delivery. In: Tissue engineering I. Springer; 2005. p. 47–90.

[31] Lee KY, Mooney DJ. Hydrogels for tissue engineering. Chemical reviews. 2001;101(7):1869–1880.

[32] Williams DF. On the mechanisms of biocompatibility. Biomaterials. 2008;29(20):2941–2953.

[33] Limpanuphap S, Derby B. Manufacture of biomaterials by a novel printing process. Journal of Materials Science: Materials in Medicine. 2002;13(12):1163–1166.

[34] Hutmacher DW. Scaffolds in tissue engineering bone and cartilage. Biomaterials. 2000;21(24):2529–2543.

[35] Zhang X, Williams D. Definitions of biomaterials for the twenty-first century. Elsevier; 2019.

[36] Pulapura S, Kohn J. Trends in the development of bioresorbable polymers for medical applications. Journal of biomaterials applications. 1992;6(3):216–250.

[37] Voytik-Harbin SL, Brightman AO, Waisner BZ, Robinson JP, Lamar CH. Small intestinal submucosa: A tissue-derived extracellular matrix that promotes tissue-specific growth and differentiation of cells in vitro. Tissue engineering. 1998;4(2):157–174.

[38] Edlund U, Albertsson AC. Degradable polymer microspheres for controlled drug delivery. In: Degradable aliphatic polyesters. Springer; 2002. p. 67–112.

[39] Van Den Bulcke AI, Bogdanov B, De Rooze N, Schacht EH, Cornelissen M, Berghmans H. Structural and rheological properties of methacrylamide modified gelatin hydrogels. Biomacromolecules. 2000;1(1):31–38.

[40] Nichol JW, Koshy ST, Bae H, Hwang CM, Yamanlar S, Khademhosseini A. Cell-laden microengineered gelatin methacrylate hydrogels. Biomaterials. 2010;31(21):5536–5544.

[41] Noshadi I, Hong S, Sullivan KE, Sani ES, Portillo-Lara R, Tamayol A, et al. In vitro and in vivo analysis of visible light crosslinkable gelatin methacryloyl (GelMA) hydrogels. Biomaterials science. 2017;5(10):2093–2105.

[42] Yue K, Li X, Schrobback K, Sheikhi A, Annabi N, Leijten J, et al. Structural analysis of photocrosslinkable methacryloyl-modified protein derivatives. Biomaterials. 2017;139:163–171.

[43] Gao G, Schilling AF, Hubbell K, Yonezawa T, Truong D, Hong Y, et al. Improved properties of bone and cartilage tissue from 3D inkjet-bioprinted human mesenchymal stem cells by simultaneous deposition and photocrosslinking in PEG-GelMA. Biotechnology letters. 2015;37(11):2349–2355.

[44] Pepelanova I, Kruppa K, Scheper T, Lavrentieva A. Gelatin-Methacryloyl (GelMA) hydrogels with defined degree of functionalization as a versatile toolkit for 3D cell culture and extrusion bioprinting. Bioengineering. 2018;5(3):55.

[45] Luo Y, Shoichet MS. A photolabile hydrogel for guided three-dimensional cell growth and migration. Nature materials. 2004;3(4):249–253.

[46] Swinehart DF. The beer-lambert law. Journal of chemical education. 1962;39(7):333.

[47] Helgason S, Helgason S. The radon transform. vol. 2. Springer; 1980.

[48] Toft PA. The Radon transform-theory and implementation. 1996;.

[49] Durrani T, Bisset D. The Radon transform and its properties. Geophysics. 1984;49(8):1180–1187.

[50] Gullberg GT. The reconstruction of fan-beam data by filtering the back-projection. Computer Graphics and Image Processing. 1979;10(1):30–47.

[51] Loterie D, Delrot P, Moser C. Volumetric 3D Printing of Elastomers by Tomographic Back-projections. Preprint. 2018;.

[52] Goetzberger A, Knobloch J, Voss B. Crystalline silicon solar cells. New York. 1998;p. 114–118.

[53] Peng Z, Hwang JY, Mouris J, Hutcheon R, Huang X. Microwave penetration depth in materials with non-zero magnetic susceptibility. ISIJ international. 2010;50(11):1590–1596.

[54] Melchiorri AJ, Fisher JP. Bioprinting of blood vessels. In: Essentials of 3D Biofabrication and Translation. Elsevier; 2015. p. 337–350.

[55] Gong J, Schuurmans CC, van Genderen AM, Cao X, Li W, Cheng F, et al. Complexation-induced resolution enhancement of 3D-printed hydrogel constructs. Nature communications. 2020;11(1):1–14.